Imaging Patterns of Toxic and Metabolic Brain Disorders

Arthur M. de Oliveira, MD
Matheus V. Paulino, MD
Ana P. F. Vieira, MD
Alexander M. McKinney, MD, CI-CIIP
Antonio J. da Rocha, MD, PhD
Germana T. dos Santos, MD
Claudia da Costa Leite, MD, PhD
Luis F. de Souza Godoy, MD
Leandro T. Lucato, MD, PhD

Abbreviations: ADC = apparent diffusion coefficient, AHE = acute hepatic encephalopathy, ATL = acute toxic leukoencephalopathy, CNS = central nervous system, DWI = diffusion-weighted imaging, FLAIR = fluid-attenuated inversion recovery, MBD = Marchiafava-Bignami disease, ODS = osmotic demyelination syndrome, PRES = posterior reversible encephalopathy syndrome, RSL = reversible splenial lesion, WE = Wernicke encephalopathy

RadioGraphics 2019; 39:1672–1695

https://doi.org/10.1148/rg.2019190016

Content Codes: ER MR NR

From the Neuroradiology Section, Institute of Radiology, Hospital das Clínicas, Faculdade de Medicina da Universidade de São Paulo (HC-FMUSP), R Dr Ovídio Pires de Campos 75, São Paulo, SP 05403-010, Brazil (A.M.d.O., M.V.P., G.T.d.S., C.d.C.L., L.F.d.S.G., L.T.L.); Neuroradiology Section, Department of Radiology, Hospital Sirio-Libanês, São Paulo, Brazil (A.P.F.V.); Neuroradiology Division, Department of Radiology, University of Minnesota Medical Center, Minneapolis, Minn (A.M.M.); and Division of Neuroradiology, Santa Casa de São Paulo School of Medical Sciences, São Paulo, Brazil (A.J.d.R.). Recipient of a Magna Cum Laude award for an education exhibit at the 2018 RSNA Annual Meeting. Received February 14, 2019; revision requested April 22 and received May 16; accepted June 24. For this journal-based SA-CME activity, the authors A.M.M. and L.T.L. have provided disclosures (see end of article); all other authors, the editor, and the reviewers have disclosed no relevant relationships. **Address correspondence to** A.M.d.O. (e-mail: *arthurmdeoliveira@gmail.com*).

Toxic and metabolic brain disorders are relatively uncommon diseases that affect the central nervous system, but they are important to recognize as they can lead to catastrophic outcomes if not rapidly and properly managed. Imaging plays a key role in determining the most probable diagnosis, pointing to the next steps of investigation, and providing prognostic information. The majority of cases demonstrate bilateral and symmetric involvement of structures at imaging, affecting the deep gray nuclei, cortical gray matter, and/or periventricular white matter, and some cases show specific imaging manifestations. When an appropriate clinical situation suggests exogenous or endogenous toxic effects, the associated imaging pattern usually indicates a restricted group of diagnostic possibilities. Nonetheless, toxic and metabolic brain disorders in the literature are usually approached in the literature by starting with common causal agents and then reaching imaging abnormalities, frequently mixing many different possible manifestations. Conversely, this article proposes a systematic approach to address this group of diseases based on the most important imaging patterns encountered in clinical practice. Each pattern is suggestive of a most likely differential diagnosis, which more closely resembles real-world scenarios faced by radiologists. Basic pathophysiologic concepts regarding cerebral edemas and their relation to imaging are introduced—an important topic for overall understanding. The most important imaging patterns are presented, and the main differential diagnosis for each pattern is discussed.

Online supplemental material is available for this article.

SA-CME LEARNING OBJECTIVES

After completing this journal-based SA-CME activity, participants will be able to:

- Identify the imaging features of some of the most prevalent CNS toxic and metabolic disorders.
- Describe imaging findings that are highly specific for the diagnosis of particular toxic and metabolic brain disorders.
- Recognize the most important types of cerebral edema and their imaging characteristics.

See rsna.org/learning-center-rg.

Introduction

This article addresses some of the most challenging diagnostic issues in neuroimaging. Toxic and metabolic brain disorders manifest secondary to derangements of a well-balanced environment encompassing metabolic substrates, neurotransmitters, electrolytes, physiologic pH levels, and blood flow, either by endogenous malfunctions or exogenous toxic effects. Patients with these disorders often present

TEACHING POINTS

- Toxic and metabolic disorders affecting the CNS usually manifest imaging characteristics and topographic distributions that should raise suspicion for such diagnoses when the clinical context is compatible. Bilateral and symmetric lesions with restricted diffusion, no or mild mass effects, and no enhancement are often depicted. In addition, sites with higher susceptibility include the cortical gray matter, deep gray nuclei, thalami, periventricular white matter, and corpus callosum. Therefore, lesions with such features and distributions can be secondary to underlying toxic effects. However, such manifestations are unspecific without adequate clinical context and can represent other conditions. Inborn errors of metabolism and hypoxia may have similar imaging features, but the presented context is usually different for these possibilities. Thus, correlations with clinical history are of particular importance in guiding imaging analysis.
- A clinical finding of acute diffuse white matter impairment corroborated by bilateral symmetric confluent areas of true restricted diffusion involving the periventricular white matter and sparing the basal ganglia at DWI signals ATL as an underlying cause. Subsequent normalization of findings is related to intramyelinic edema.
- Common sites involved in WE include the regions surrounding the third ventricle (the medial thalami in 85% of cases, the mammillary bodies in 60% of cases, and the hypothalamus), the tectal plate and the periaqueductal gray matter in two-thirds of cases, and the putamina.
- In nearly all cases of metronidazole-induced brain toxicity (up to 93%), MR images show bilateral symmetric lesions in the cerebellum, particularly involving the dentate nuclei. A majority of cases (86%) show a characteristic pattern of bilateral symmetric involvement of the dentate nuclei, vestibular nuclei, tegmenta, and superior olivary nuclei.
- ODS affecting extrapontine cerebral regions, including the cortex, has been extensively described. Approximately 50% of cases manifest isolated pontine lesions, with pontine and extrapontine lesions in 30% of cases. There are only extrapontine lesions in 20% of ODS cases, which makes diagnosing this condition even more challenging and underscores the importance of recognizing the spectrum of ODS symptoms.

to the emergency department and are diagnosed with global cerebral dysfunction presenting as acute confusional state and delirium, but commonly they are also critically ill inpatients. These cases often demand a fast and effective management approach because they may result in permanent structural brain damage. Imaging plays a key role in these cases, as imaging findings can be used to diagnose the condition or narrow the differential diagnosis (1).

In addition to providing a final diagnosis, imaging can provide prognostic information. Extensive lesions involving gray matter are often related to poor prognosis and outcomes, while lesions restricted to white matter, sparing cortical and deep gray matter, can point to a reversible cause.

Toxic and metabolic disorders affecting the central nervous system (CNS) usually manifest imaging characteristics and topographic distributions that should raise suspicion for such diagnoses when the clinical context is compatible. Bilateral and symmetric lesions with restricted diffusion, no or mild mass effects, and no enhancement are often depicted. In addition, sites with higher susceptibility include the cortical gray matter, deep gray nuclei, thalami, periventricular white matter, and corpus callosum. Therefore, lesions with such features and distributions can be secondary to underlying toxic effects. However, such manifestations are unspecific without adequate clinical context and can represent other conditions. Inborn errors of metabolism and hypoxia may have similar imaging features, but the presented context is usually different for these possibilities. Thus, correlations with clinical history are of particular importance in guiding imaging analysis. By allying imaging patterns with some clinical findings, it is possible to reach a hypothesis with good accuracy (2).

The brain is highly susceptible to a number of acquired metabolic abnormalities, and the list of toxins and poisons that affect the CNS is long (Table 1). Some agents accumulate slowly such that their clinical manifestations are insidious, while others cause profound almost immediate CNS toxic effects. Aiming at a more practical and easier line of attack to address this group of diseases, this article proposes an approach

Table 1: Major Causes of Toxic and Metabolic Disorders

Most common endogenous metabolic derangements related to CNS involvement
Hypertensive encephalopathies
Glucose disorders
Parathyroid disorders
Hepatic encephalopathy (manganese and/or ammonia levels)
Uremic encephalopathy
ODS
Cobalamin deficiency
Major exogenous causes of toxic encephalopathy
Alcohol-related disorders (WE, MBD)
Industrial agents (methanol, toluen)
Inhaled gases (carbon monoxide, pesticides)
Illicit drug use (heroin, cocaine)
Chemotherapeutic agents (methotrexate, fludarabine, 5-fluorouracil)
Immunosuppressive agents (TNF-α blockers, cyclosporine)
Other potentially neurotoxic medications (metronidazole, vigabatrine)

Note.—MBD = Marchiafava-Bignami disease, ODS = osmotic demyelination syndrome, TNF = tumor necrosis factor, WE = Wernicke encephalopathy.

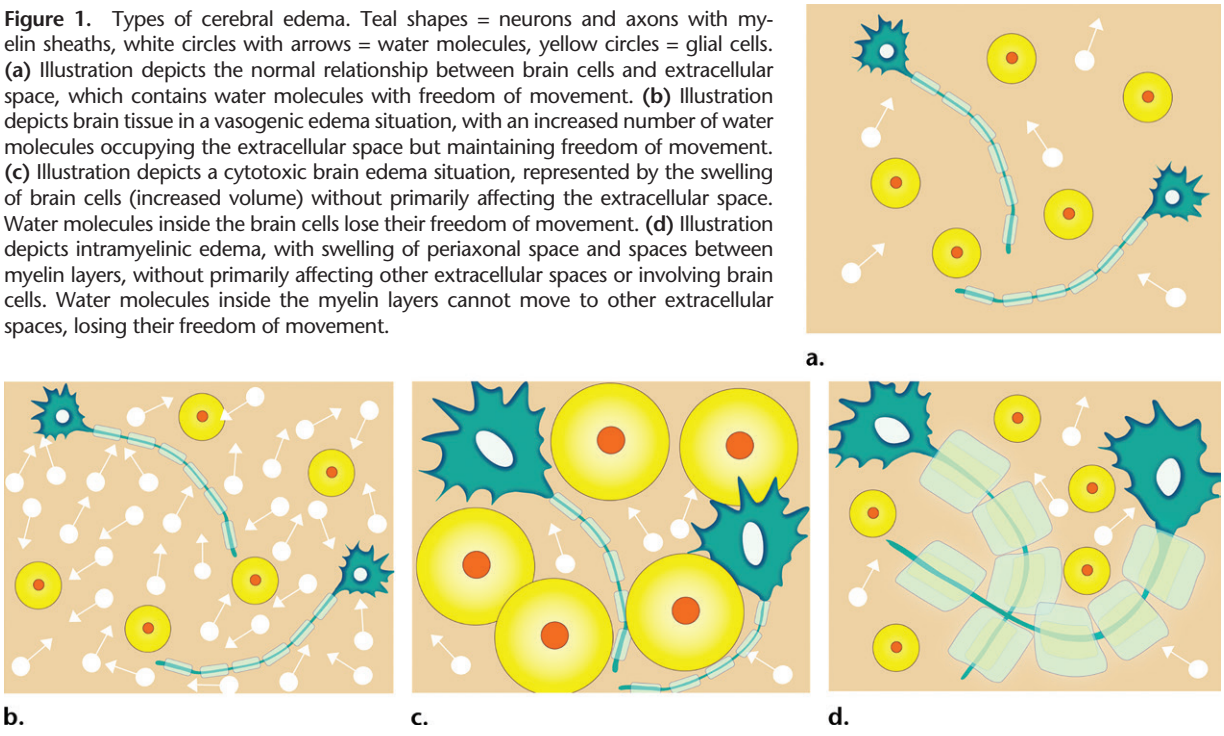

Figure 1. Types of cerebral edema. Teal shapes = neurons and axons with myelin sheaths, white circles with arrows = water molecules, yellow circles = glial cells. **(a)** Illustration depicts the normal relationship between brain cells and extracellular space, which contains water molecules with freedom of movement. **(b)** Illustration depicts brain tissue in a vasogenic edema situation, with an increased number of water molecules occupying the extracellular space but maintaining freedom of movement. **(c)** Illustration depicts a cytotoxic brain edema situation, represented by the swelling of brain cells (increased volume) without primarily affecting the extracellular space. Water molecules inside the brain cells lose their freedom of movement. **(d)** Illustration depicts intramyelinic edema, with swelling of periaxonal space and spaces between myelin layers, without primarily affecting other extracellular spaces or involving brain cells. Water molecules inside the myelin layers cannot move to other extracellular spaces, losing their freedom of movement.

beginning with a given general imaging pattern and discussing its most important possible differential diagnoses, highlighting imaging findings or clinical information that can lead to a specific diagnosis.

Cerebral Edema

Vasogenic and cytotoxic edema have been traditionally related to alterations encountered in toxic and metabolic brain disorders. Each one encompasses many causes that share similar interconnected processes resulting in abnormal shifts in water among various compartments of the brain parenchyma. Each type of cerebral edema leads to particular imaging findings. Recently, other pathologic concepts have been used in neuroimaging to describe and explain some specific imaging findings and disorders, such as the concepts of excitotoxic injury and intramyelinic edema (3,4). Figure 1 depicts a schematic representation of the most important alterations affecting brain tissue in each type of edema.

Vasogenic cerebral edema refers to a process induced by mechanical or chemical insults that leads to blood-brain barrier disruption, whether by physical damage or endothelial activation by blood mediators, resulting in leakage of fluid from capillaries into the extracellular space in the white matter. Images show T2-weighted and fluid-attenuated inversion-recovery (FLAIR) hyperintensities owing to water accumulation in the extracellular space, without restricted diffusion, as the freedom of movement of water molecules is not affected. Vasogenic edema can produce mass effect, with dislocation of structures and defacement of the cerebral sulci. The gray matter is maintained, as this type of edema mainly involves the white matter, extending in a fingerlike fashion. Common examples include edemas associated with tumors and abscesses, as well as posterior reversible encephalopathy syndrome (PRES) (3,4).

Cytotoxic cerebral edema, the classic edema associated with cerebral ischemia, is a condition in which extracellular water passes into cells, causing them to swell. In brief, prior ischemic or hypoxic insults impair mitochondrial function and adenosine triphosphate production and cause failure of ion pumps and accumulation of metabolites (such as lactate), resulting in cellular edema. This process does not compromise the blood-brain barrier and mainly affects gray matter, although white matter is also involved. The imaging features of cytotoxic cerebral edema appear primarily as changes at diffusion-weighted imaging (DWI) caused by restricted water diffusivity within brain cells, without T1- or T2-weighted changes, as the entire process is a redistribution of water. Importantly, the changes are not completely reversible (cell death), and as the pathologic process progresses, alterations in T2-weighted signal intensity and contrast enhancement can appear secondarily (3,4).

Excitotoxic brain injury is a final common pathway of many cerebral disorders, such as infarction, hypoxic-ischemic encephalopathy, and status epilepticus, but it is also closely related to

Table 2: Most Common Causes of ATL

Chemotherapeutic agents (methotrexate, fludarabine)
Opioid use (heroin, opiates)
AHE
Immunosuppressive agents (cyclosporine, tacrolimus)
Carbon monoxide poisoning (subacute presentation)
Other (uremia, cocaine use, metronidazole use)

Note.—AHE = acute hepatic encephalopathy.

toxic and metabolic disorders. Excitotoxicity is the excessive release of excitatory amino acids in the synaptic cleft, with glutamate being the most important neurotransmitter responsible for many neurologic functions (memory, cognition, movement, and sensation). Excessive glutamate in the synaptic cleft can lead to cell swelling and subsequent death (ie, cytotoxic edema) in the event of ischemia and cell failure with disruption of glutamate reuptake. If the reuptake of glutamate is maintained, cell swelling and death may not occur. Instead, the process known as intramyelinic edema may occur instead.

The myelin sheath is composed of layers of myelin around axons that form tight junctions with axons and isolate the periaxonal space and spaces between myelin layers from other extracellular spaces. Such sites are virtual but potential extracellular spaces. Thus, intramyelinic edema refers to non-neurotoxic edema in these virtual spaces, which is characterized by restricted diffusion (as water molecules are unable to shift to other extracellular spaces) and reversibility of the condition (without cell death). Consequently, the imaging hallmark is true and reversible diffusion-weighted restriction. It is believed that intramyelinic edema alone results in completely reversible edema, while irreversible or partially reversible conditions manifest when cellular edema is concurrently present. The periventricular white matter and the splenium, which are known to have higher metabolism, are especially susceptible to these changes (5,6).

Imaging Patterns

Toxic and metabolic disorders are closely related to excitotoxic brain injury, as they often induce intense glutamate release. Although receptors related to excitotoxic injury are widely distributed in the brain, there are classic CNS sites that are particularly susceptible to this mechanism, such as the basal ganglia and thalami, cortical gray matter, periventricular white matter, and the corpus callosum. This differential susceptibility is important because it indicates some possible characteristic imaging patterns that could lead to the consideration of toxic and metabolic causes during diagnosis (5–7).

Another important concept to be introduced is acute toxic leukoencephalopathy (ATL). ATL, which has been recently described in terms of its clinical, radiologic, and pathologic features, relates to cerebral white matter alterations secondary to various toxic agents and has great potential for reversibility if rapidly and correctly approached, highlighting the importance of its recognition (8). A clinical finding of acute diffuse white matter impairment corroborated by bilateral symmetric confluent areas of true restricted diffusion involving the periventricular white matter and sparing the basal ganglia at DWI signals ATL as an underlying cause. Subsequent normalization of findings is related to intramyelinic edema, as described previously (8,9). Table 2 summarizes the most common causes of ATL.

Toxic and metabolic disorders affecting the CNS are usually depicted on images following some patterns of involvement that are closely related to the pathophysiologic mechanism of damage, which is important to recognize because each pattern can point to a most likely diagnosis and even indicate the prognosis. Note that each pattern indicates the most commonly involved sites for a group of diseases but each disease can manifest more than one pattern and can affect other structures. The most important patterns are as follows (Fig 2):

1. Basal ganglia and/or thalami involvement. The periventricular white matter and the cortical gray matter may be also involved. This pattern is usually related to cytotoxic brain edema, poor outcomes, and irreversibility.
2. Dentate nuclei involvement.
3. Prominent cortical gray matter involvement. Although cortical lesions can coexist with basal ganglia- and white matter–associated involvement, they are the most distinguishing feature.
4. Symmetric periventricular white matter involvement with gray matter sparing. This is a pattern that includes ATL causes and is more related to intramyelinic edema and higher possibilities of reversibility and better outcomes.
5. Corticospinal tract region involvement.
6. Corpus callosum involvement.
7. Asymmetric white matter involvement in a demyelinating disease pattern.
8. Parieto-occipital subcortical vasogenic edema.
9. Central pons involvement.

The pattern of involvement, damage extension, and possibility of reversion (mainly in cases of ATL) are related primarily to the

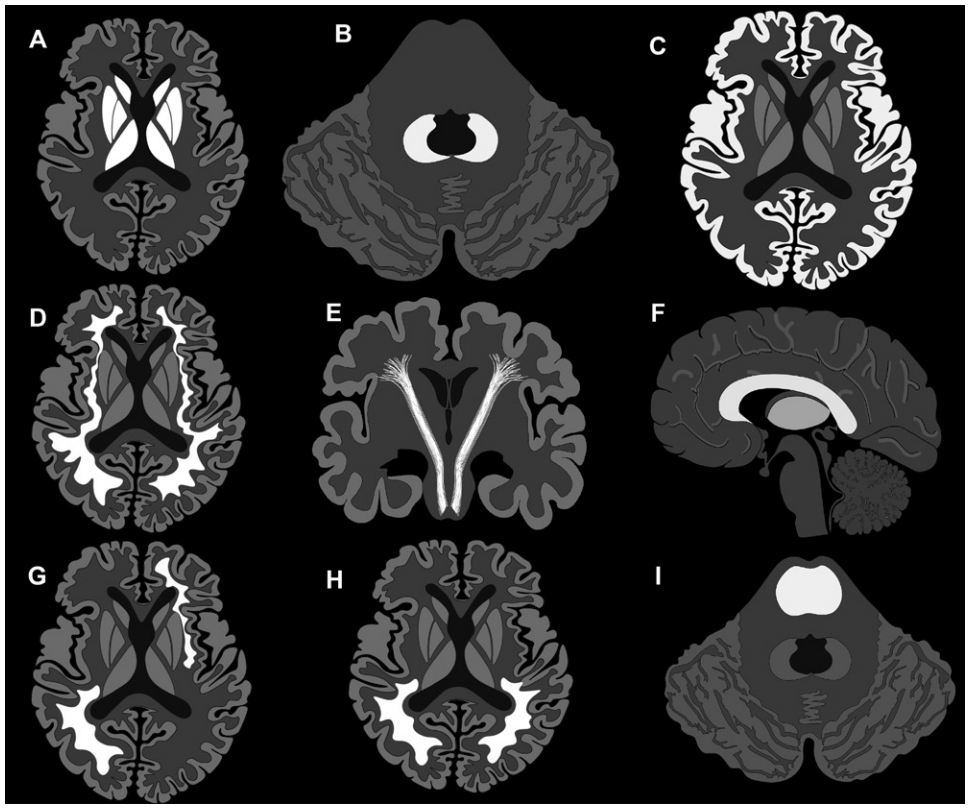

Figure 2. Illustration shows the most important general imaging patterns in toxic and metabolic brain disorders. White areas = areas of involvement. These include symmetric basal ganglia and/or thalami involvement (axial view) *(A)*; symmetric dentate nuclei involvement (axial view) *(B)*; prominent cortical gray matter involvement (axial view) *(C)*; symmetric periventricular white matter involvement (with gray matter sparing) (axial view) *(D)*; corticospinal tract involvement (axial view) *(E)*; corpus callosum involvement (coronal view) *(F)*; asymmetric white matter involvement (demyelinating disease pattern) (axial view) *(G)*; parieto-occipital subcortical vasogenic edema (axial view) *(H)*; and central pons involvement (axial view) *(I)*.

intensity and duration of exposure to a determined agent (2,7–9).

Keep in mind that such patterns of involvement are unspecific and comprise various possible diagnoses, but they can be used as a guide since each pattern is related to a minor number of diagnostic possibilities and can be a prognostic factor.

Pattern 1: Basal Ganglia and/or Thalami Involvement

Pattern 1a: T2-weighted and FLAIR Hyperintensity

Wernicke Encephalopathy.—WE is usually related to chronic and frequent alcohol intake, but it is important to remember that almost 50% of WE cases are unrelated to alcohol use (10). The underlying pathophysiology is associated with nutritional deficiencies, notably thiamine (vitamin B1). Thiamine is important in maintaining osmotic gradients across the cell membrane, ensuring its integrity (2).

Aside from alcohol abuse, other important causes of WE include hyperemesis (pregnancy-related, chemotherapy), eating disorders, and bariatric surgery, any of which can lead to secondary malnutrition (2,10,11). Although most cases occur in adults, it is important to emphasize that WE can also occur in children (2). The classic clinical triad of symptoms, including ocular dysfunction (nystagmus, ophthalmoplegia), ataxia, and confusion, manifests in only 30% of patients (11).

Imaging plays an important role in early WE diagnosis. MRI is much more sensitive than CT for evaluating alterations related to WE. Importantly, remember that cerebral atrophy and microhemorrhages can manifest owing to chronic alcohol intake. During the acute phase, symmetric bilateral T2-weighted and FLAIR hyperintensities and restricted diffusion can be observed in affected areas, with 50% of cases showing enhancement following the administration of contrast material (postcontrast). Common sites involved in WE include the regions surrounding the third ventricle (the medial thalami in 85% of cases, the mammillary bodies in 60% of cases, and the hypothalamus), the tectal plate and the periaqueductal gray matter in two-thirds of cases, and the putamina (Fig 3) (2,10,11). Other sites that can be altered, albeit less

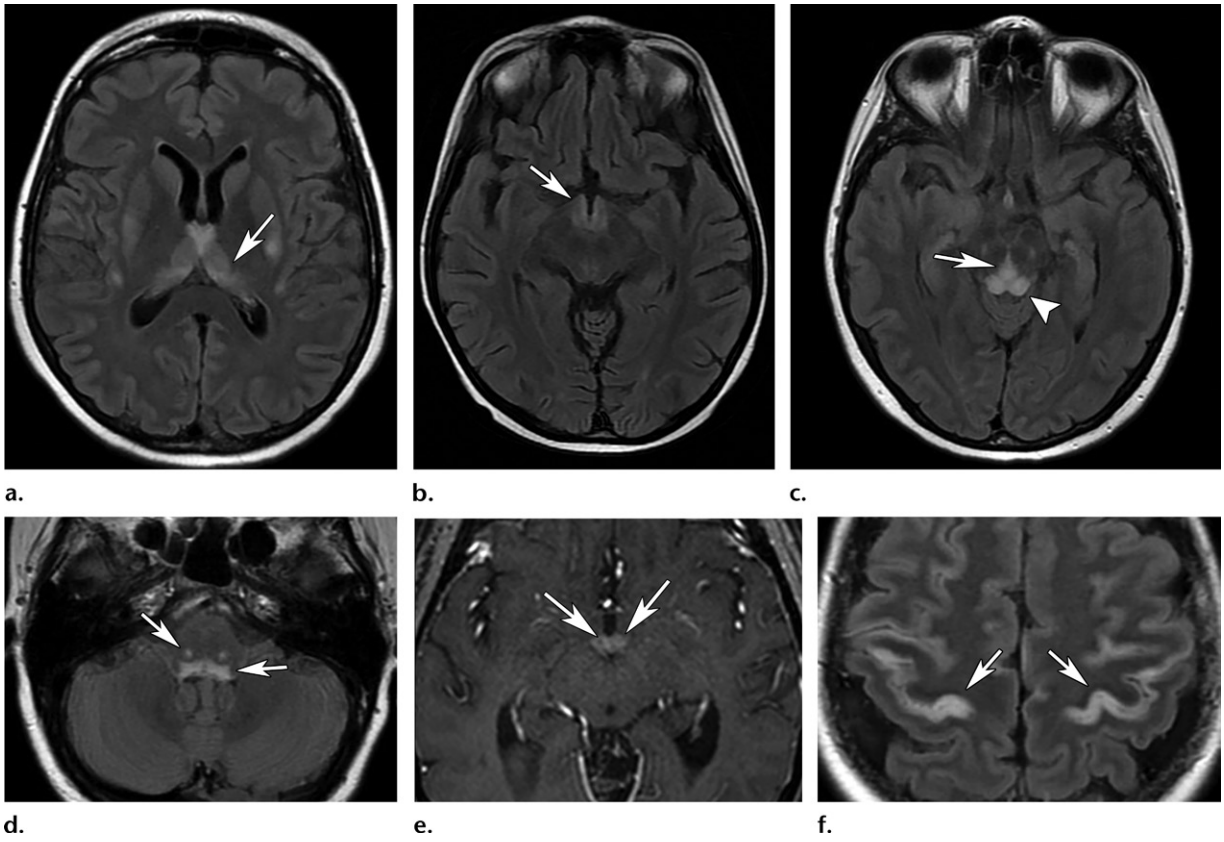

Figure 3. WE in a patient with diplopia and impaired mental status after long-term parenteral nutrition. **(a–d)** Axial FLAIR MR images show bilateral and symmetric hyperintensities involving the medial thalamus (arrow in **a**), hypothalamus (arrow in **b**), periaqueductal gray matter (arrow in **c**), tectum (arrowhead in **c**), and dorsal pons (arrows in **d**). **(e)** Axial contrast-enhanced T1-weighted MR image shows symmetric enhancement of the mammillary bodies (arrows). **(f)** Axial FLAIR MR image shows perirolandic cortical involvement (arrows).

commonly, are the dorsal medulla, cerebellum, and cranial nerve nuclei. There may also exist cortical involvement, which can be asymmetric and usually involves the perirolandic cortex (Fig 3f) (2,10,11). Strong uniform postcontrast enhancement of the mammillary bodies is observed in up to 80% of cases and is considered a pathognomonic finding for WE (Fig 3e). In the chronic phase, the mammillary bodies are atrophied (2,10,11).

Methanol Poisoning.—Methanol is a strong CNS depressant and a common component in solvents, perfumes, paint removers, and gasoline mixtures. This substance can be accidentally inhaled or ingested, with some cases of methanol poisoning resulting from the intake of adulterated alcoholic drinks (moonshine) (2,12,13).

Methanol causes severe metabolic acidosis, with patients commonly presenting in a comatose state after preceding visual and gastrointestinal symptoms. Diagnosis is often delayed, contributing to the high mortality of this condition. Important clinical clues include an increased anion gap and a latent period between ingestion and clinical symptom onset (ethanol ingested simultaneously slows methanol metabolism). Imaging can play an important role in making this diagnosis (2,12–14).

Bilateral symmetric basal ganglia necrosis is the most characteristic imaging feature of methanol poisoning. Selective or predominant involvement of the putamina with relative sparing of the globi pallidi is suggestive of methanol poisoning (Fig 4). Variable degrees of subcortical white matter and cerebellar involvement and optic nerve necrosis are depicted, dependent on the severity of the intoxication (12–14). Hemorrhagic necrosis appears as an area of hyperattenuation on CT images. MR images show T2-weighted and FLAIR hyperintensity, and susceptibility-weighted imaging sequences sometimes show associated changes owing to the presence of hemorrhage (sometimes occurring during the evolution of the disease and not in the acute phase). Restricted diffusion is depicted in the acute phases, and MR spectroscopy shows reduced *N*-acetylaspartate and elevated lactate peaks (Fig 4e) (2,12–14).

Carbon Monoxide Poisoning.—Carbon monoxide is an odorless and colorless gas usually produced by the incomplete combustion of fuels and can cause poisoning by accidental inhalation. The

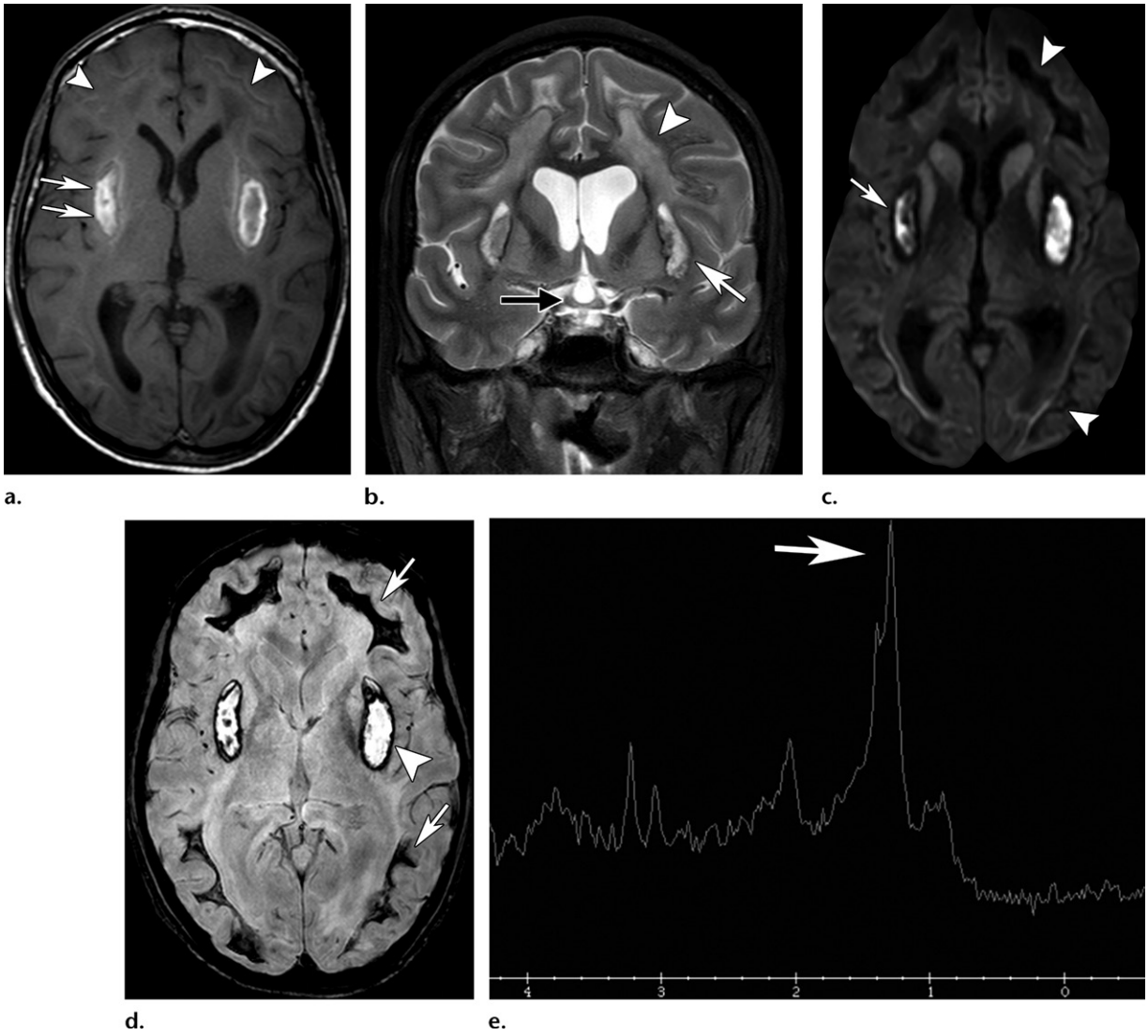

Figure 4. Methanol poisoning after moonshine intake. **(a)** Axial T1-weighted MR image shows hyperintensities involving the putamina (arrows) owing to necrotic hemorrhage. Note the subtle hyperintensities (arrowheads) involving the anterior and posterior white matter. **(b)** Coronal T2-weighted MR image shows chiasma involvement (black arrow) in addition to putamina (white arrow) and diffuse white matter (arrowhead) hyperintensities. **(c)** Axial diffusion-weighted MR image shows restricted diffusion involving the putamina (arrow). There are magnetic susceptibility artifacts involving the white matter owing to hemorrhage (arrowheads). **(d)** Axial T2*-weighted MR image shows necrotic hemorrhage, which is better demonstrated than on **b**, characterized by a rim of low signal intensity involving the putamina (arrowhead) and extensive low signal intensity involving the anterior and posterior white matter (arrows). **(e)** MR spectroscopic image with short echo time shows a huge lactate peak at 1.3 ppm (arrow).

toxic mechanism is secondary to impaired oxygen transportation, as carbon monoxide combines with hemoglobin with over 200 times higher affinity than that of oxygen (2,15,16).

Because the globus pallidus is sensitive to hypoxia, its bilateral symmetric necrotic involvement is the hallmark of carbon monoxide poisoning (Fig 5). Hypoattenuation in both globi pallidi can be visualized on CT images, with hyperintensities on T2-weighted and FLAIR images and a thin hypointense rim around the lesion caused by hemorrhage (hyperintense on T1-weighted images). Diffusion-weighted images show restricted diffusion, and susceptibility-weighted sequences may show areas of hypointensity corresponding to hemorrhage (2,15). In addition to the globi pallidi, less common sites that may be involved are the hippocampi, caudate nuclei, putamina, thalami, cerebellum, corpus callosum, and cerebral cortex (2,15,16).

The second most commonly affected site is the cerebral white matter (up to one-third of patients), which can show delayed leukoencephalopathy in the subacute phase of carbon monoxide poisoning. This effect, which appears weeks after the initial insult, is characterized by progressive white matter demyelination with extensive bilateral symmetric confluent areas of hyperintensity on T2-weighted and FLAIR images and subsequent (months later) complete or partial resolution (Fig 5) (2,17).

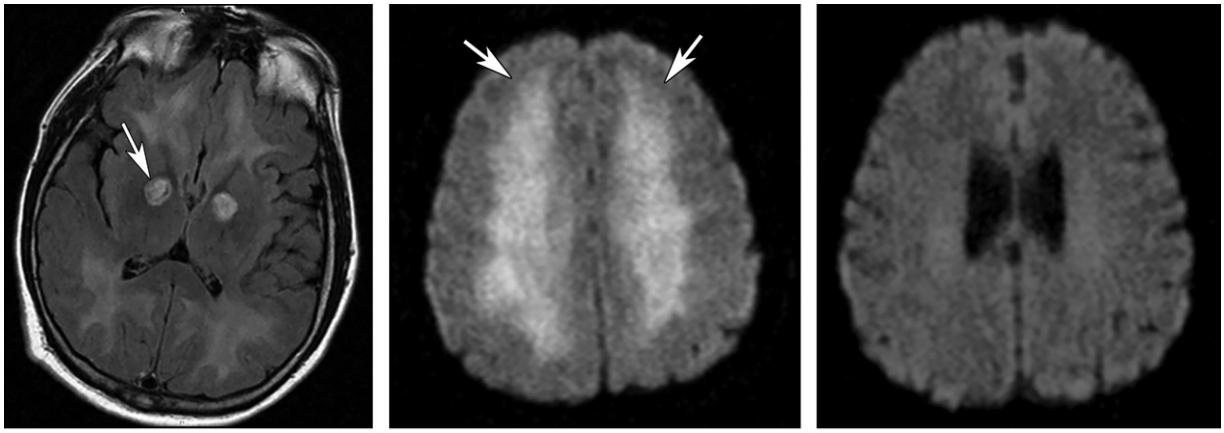

a. b. c.

Figure 5. Carbon monoxide poisoning in two patients. **(a)** Axial FLAIR MR image shows symmetric hyperintensity involving both globi pallidi (arrow) and sparing the putamina, a classic finding of this condition. Note that there is also white matter involvement. **(b, c)** Axial diffusion-weighted MR images in another patient show subacute extensive bilateral and symmetric areas of restricted diffusion involving the periventricular white matter (arrows in **b**), with posterior normalization on the 1-year follow-up image **(c)**.

At that point, it is important to remember the importance of correlation with clinical history, as some conditions may mimic carbon monoxide poisoning with bilateral globi pallidi involvement, such as hypoxic-ischemic encephalopathy and drug use (15,16).

Vigabatrin-associated Toxicity.—Vigabatrin is an antiepileptic drug used for the treatment of infantile spasms. The potential risk of developing brain abnormalities during the course of treatment is well known. Approximately one-third of patients develop such abnormalities, with little variation among current studies (17,18). The younger the patient, the higher the risk, with patients younger than 1 year being the most commonly affected (17,18).

Important characteristics of this entity are a frequently asymptomatic course and reversibility through drug discontinuation. Recent studies demonstrate that affected children received higher doses than unaffected children, but the duration of treatment was not an important factor (17,18).

Images depict classic findings of toxic encephalopathy, with symmetric restricted diffusion and T2-weighted and FLAIR hyperintensity in involved areas, subsequently normalized after vigabatrin withdrawal. The major affected areas are the globi pallidi, thalami, dorsal brainstem, and dentate nuclei (Fig 6) (17,18).

Uremic Encephalopathy.—Uremic encephalopathy, a metabolic disorder that occurs in the context of both acute and chronic renal failure, is a complication resulting from the presence of endogenous uremic toxins in patients with severe renal failure. The pathogenesis is complex and unclear, and the condition is likely caused by the effects of neurotoxicity from the accumulation of uremic toxins such as guanidine compounds (19–21). Clinical manifestations include various neurologic symptoms, such as movement disorders (tremor, asterixis, myoclonus), seizures, cognitive disorders, and impaired mental status (21).

Uremic encephalopathy has three patterns of imaging findings: basal ganglia involvement (most common), cortical or subcortical involvement (PRES-like), and white matter involvement (caused by ATL). Imaging findings are unspecific, and the patient's clinical history and laboratory findings are indispensable for diagnosis. Imaging can also aid in clinical management because it can shed light on the severity and possible reversibility.

The most common finding is bilateral symmetric involvement of the basal ganglia with variable white matter and cortical-associated involvement (19,20). The lentiform fork sign can be identified in patients with uremic encephalopathy and may be indicative of underlying metabolic acidosis coexisting with uremia, a typically encountered association. This sign is characterized on T2-weighted and FLAIR images by hyperintensity of the white matter that surrounds the lentiform nuclei (internal and external capsules and the medullary laminae), delineating the lateral and medial boundaries of both putamina, giving its peculiar appearance that is more commonly found in patients with diabetes (Fig 7) (19,22).

Pattern 1b: T2 Hypointensity

Toluene Use.—Toluene is the most important component of industrial solvents. This lipid-soluble product, found in glues, paint thinners, and inks, can be rapidly absorbed by the CNS. Clinical and imaging findings usually manifest

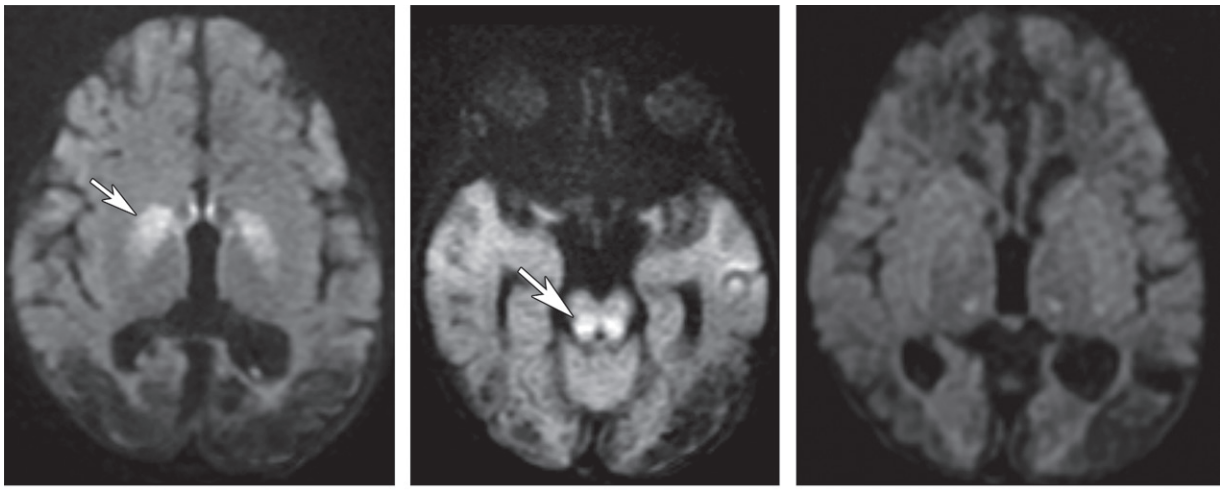

a. b. c.

Figure 6. Vigabatrin-associated toxicity. Axial diffusion-weighted MR images show restricted diffusion symmetrically involving the globi pallidi (arrow in **a**) and dorsal brainstem (arrow in **b**), with normalization on the 6-month follow-up image **(c)**.

after chronic use (years), and thus the condition is termed *chronic solvent encephalopathy* (2,23,24).

Continued toluene use leads to severe irreversible cognitive impairment, which is an important clue for diagnosis in adolescents and young adults because this population is not usually affected by dementia, and toluene use is widespread in this population. Alterations depicted on images include diffuse periventricular white matter lesions that are hyperintense on T2-weighted and FLAIR images and significant T2 hypointensity involving the thalami, basal ganglia, and substantiae nigrae (Fig 8) (23,24). The cause for such hypointensity is still not known. It has been hypothesized to be secondary to excessive iron deposition (25). Generalized cerebral and cerebellar atrophy also manifest, with ventricular dilatation and thinning of the corpus callosum (2).

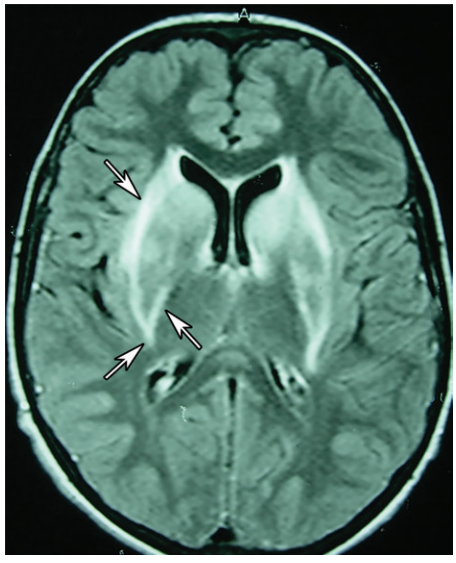

Figure 7. Uremic encephalopathy. Axial FLAIR MR image shows symmetric involvement of the basal ganglia, with hyperintensities (arrows) affecting the white matter that surrounds the basal ganglia, delineating the lateral and medial boundaries of both putamina (ie, lentiform fork sign).

***Parathyroid-Hypofunction Disorders and Hyperparathyroidism-related Disorders*—**Parathyroid-hypofunction disorders are characterized by hypofunction of the parathyroid glands or their products. There are three main types, differentiated by clinical and laboratory findings: *(a)* hypoparathyroidism, *(b)* pseudohypoparathyroidism, and *(c)* pseudopseudohypoparathyroidism (2,26).

The main imaging findings are the same for all conditions and are related to calcium deposition in the basal ganglia. CT images show coarse bilateral and symmetric calcifications in the globi pallidi, putamina, and caudate nuclei, emphasizing that the thalami, subcortical white matter, and dentate nuclei may also be affected (Fig 9). MR images can depict hyperintensity on T1-weighted images and hypointensity on T2-weighted images. T2*- or susceptibility-weighted images can depict blooming artifacts related to calcium deposition (2,26).

An important differential diagnosis is Fahr disease, a genetic condition characterized by idiopathic basal ganglia calcification with a similar imaging pattern to that of parathyroid-hypofunction disorders but without laboratory alterations (2).

Disorders related to hyperparathyroidism are characterized by hyperfunction of the parathyroid glands or high serum levels of parathyroid hormone. Primary hyperparathyroidism is caused by parathyroid adenoma (75%–85%), parathyroid hyperplasia (10%–20%), or carcinoma (1%–5%) and is characterized by high serum levels of

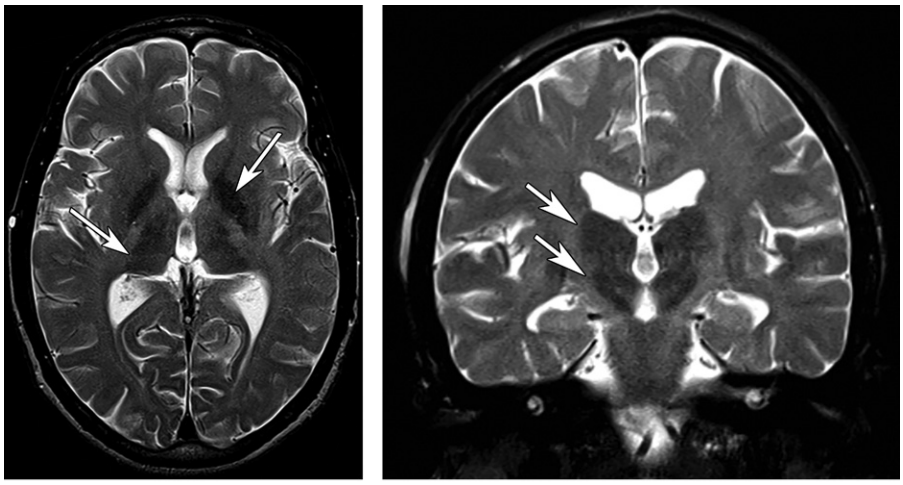

Figure 8. Effects of chronic toluene use. **(a)** Axial T2-weighted MR image shows accentuated symmetric hypointensities (arrows) involving the globi pallidi and thalami. **(b)** Coronal T2-weighted MR image shows symmetric hypointensities (arrows) involving the thalami and substantiae nigrae.

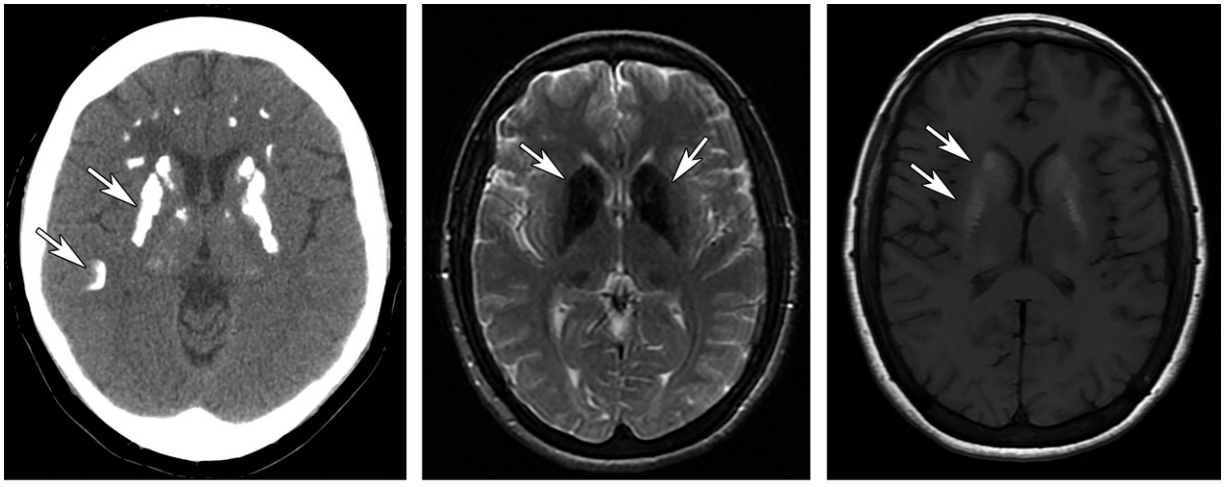

Figure 9. Primary hypoparathyroidism in a 10-year-old boy who presented with tetany and hyperreflexia and was diagnosed with concomitant low levels of calcium and parathyroid hormone. **(a)** Axial CT image (soft-tissue window) shows coarse and symmetric calcifications (arrows) in the basal ganglia and periventricular white matter. **(b, c)** Axial T2-weighted **(b)** and T1-weighted **(c)** MR images show low-signal-intensity abnormalities in **b** and high-signal-intensity abnormalities in **c**, involving the basal ganglia produced by the calcifications (arrows).

parathyroid hormone and calcium serum levels. Secondary hyperparathyroidism is related to chronic renal failure, in which the kidneys fail to convert vitamin D to the active form and excrete phosphate, leading to high parathyroid hormone levels, normal or low calcium levels, and high phosphate serum levels (2,27,28).

In hyperparathyroid disturbances, as in hypoparathyroid disorders, bilateral symmetric calcifications are depicted in the basal ganglia. In primary hyperparathyroidism, the salt-and-pepper appearance (ie, multiple well-defined hypointensities in the skull owing to trabecular bone resorption) can be observed, while in secondary hyperparathyroidism, diffuse thickening of the skull, plaquelike dural thickening, calcification, and pipestem calcifications of carotid arteries are found. Brown tumors can manifest in both types of hyperparathyroidism and are described as well-defined round lytic lesions without sclerotic margins or cortical involvement (27,28).

Pattern 1c: T1 Hyperintensity

Diabetic Striatopathy.—Diabetic striatopathy is also known as *hyperglycemia-induced hemichorea-hemiballismus,* and patients with this condition present with characteristic involuntary nonpatterned movements. This is a nonketotic delayed hyperglycemia complication and can sometimes lead to a diagnosis of diabetes mellitus type 2. At presentation, the mean age is 71 years, and the mean glycemia level is 431 mg/dL (2,29,30). Nevertheless, it must be noted that symptoms of this condition can manifest acutely or even weeks after normalization of the hyperglycemic event (2,29).

Imaging findings are virtually pathognomonic and depict a usually unilateral T1 hyperintensity involving the striatum and hyperattenuation in the same region on CT images (Fig 10). Diabetic striatopathy is completely reversible in 73% of patients (29,30).

Chronic Hepatic Encephalopathy.—Chronic hepatic encephalopathy is a potentially reversible clinical syndrome that occurs in the context of chronic severe liver dysfunction. Most patients have a long history of cirrhosis accompanied by portal hypertension or portosystemic shunting (2,31,32). Neurotoxic substances accumulate within brain tissue, and manganese is the substance most related to alterations, usually observed in chronic hepatic encephalopathy (31).

Patients may have no clinical findings or only subtle cognitive and motor impairment, but they can also present with periods of decompensation of symptoms during the course of the disease that are more related to higher ammonia levels and acute hepatic encephalopathy (32).

The characteristic imaging finding is bilateral and symmetric T1 hyperintensity involving the globi pallidi and substantiae nigrae (reported in 80%–90% of patients with chronic liver failure), most likely due to manganese accumulation (Fig 11a). High signal intensity on T1-weighted images of the pituitary gland and the hypothalamus can be depicted but is less common. After liver transplant, changes can decrease or even disappear, typically normalizing after 1 year (2,31,32).

Patients receiving total parenteral nutrition, patients with occupational exposure to manganese from welding, and those with noncirrhotic portal vein thrombosis can also demonstrate similar imaging findings (32). Notably, such patients may may show glutamine-glutamate peak at MR spectroscopy with short echo times, resonating at 2.1–2.4 ppm, which is probably related to chronic accumulation of glutamine levels in the brain tissue owing to recurrent alterations in ammonia levels in chronic hepatic disease. The conversion of glutamate and ammonia into glutamine serves as a method of ammonia detoxication (32,33).

Recent studies have noted signs of brain edema, even in cases of chronic hepatic encephalopathies. Excess glutamine in cerebral tissue leads to the edema of astrocytes. For this reason, fast FLAIR sequences can show bilateral vasogenic edema (without restriction at DWI) in cerebral white matter, mainly involving the corticospinal tract (Fig 11b) (31,32).

On T2-weighted images, laminar hyperintensities involving the deep layers of perirolandic cortices have been histologically related to chronic hepatic encephalopathy. It is well known that similar cortical laminar T2 hyperintensities are also depicted in cases of hypoxic-ischemic brain injury. In hypoxic-ischemic encephalopathy, however, these are frequently located in the boundary zones of the cerebral cortices, reflecting the influence of hemodynamic factors, whereas in chronic hepatic encephalopathy these are most striking in the superior parietal and posterior frontal convexities (Fig 11c) (34).

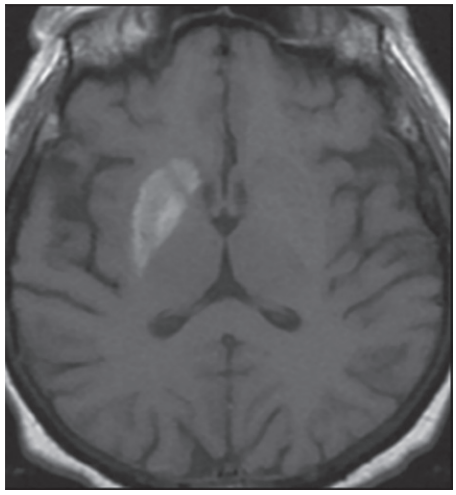

Figure 10. Diabetic striatopathy (hyperglycemia-induced hemichorea hemiballismus). Axial T1-weighted MR image shows unilateral hyperintensity in the striatum. CT images showed hyperattenuation in the same region (not shown).

Parathyroid-Related Disorders.—T1 hyperintensities involving the basal ganglia, thalami, and dentate nuclei may be secondary to calcifications (Fig 9c). In such cases, calcium metabolism disorders are more likely to have manifested (2).

Figure E1 summarizes the disorders associated with pattern 1.

Pattern 2: Dentate Nuclei Involvement

Metronidazole-induced Brain Toxicity

Metronidazole is an antibiotic that is used to treat a wide variety of bacterial and protozoal infections and was recently reported to rarely cause CNS toxic effects. These toxic effects can affect patients of all ages, usually appearing during prolonged treatment, frequently over 25 days of use (mean duration, 54 days), but it is important to emphasize that shorter periods, such as 7 days, have also been described to cause such toxic effects (35,36).

Patients present with symptoms of cerebellar dysfunction, such as dysarthria, ataxia, and dysmetria (75% of cases), confusion (33%), and seizures (13%) (35).

In nearly all cases of metronidazole-induced brain toxicity (up to 93%), MR images show

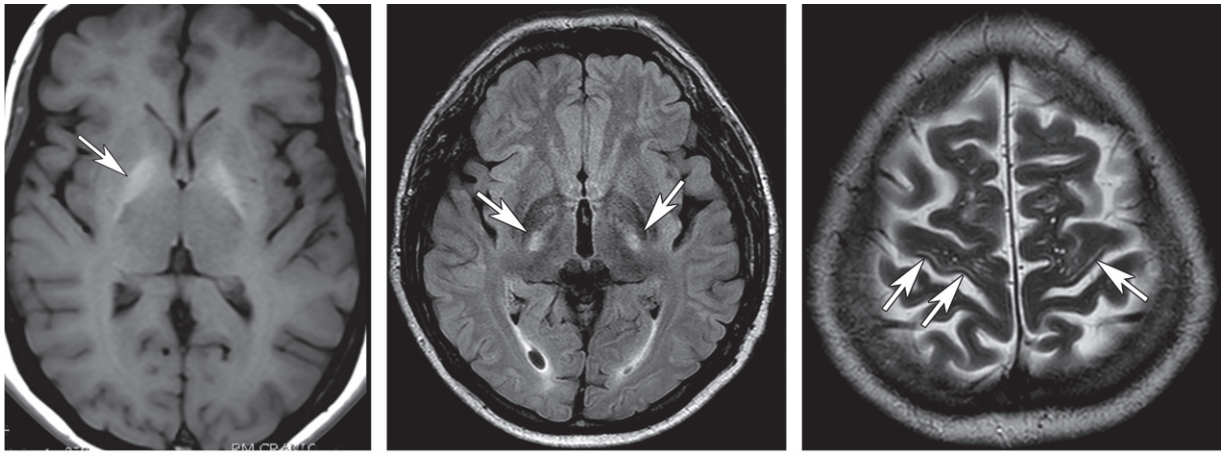

a. b. c.

Figure 11. Chronic hepatic encephalopathy. **(a)** Axial T1-weighted MR image shows symmetric hyperintensity (arrow) involving the globi pallidi. **(b)** Axial FLAIR MR image shows high-signal-intensity abnormalities (arrows) along the corticospinal tracts, at the level of the posterior limb of the internal capsule. **(c)** Axial T2-weighted MR image shows linear hyperintensities (arrows) involving the deep layers of the perirolandic cortex.

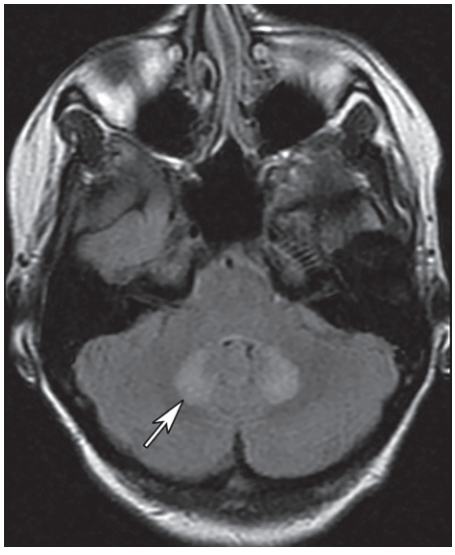

Figure 12. Metronidazole-induced brain toxicity. Axial FLAIR MR image shows a symmetric hyperintensity (arrow) involving the dentate nuclei.

bilateral symmetric lesions in the cerebellum, particularly involving the dentate nuclei (Fig 12). A majority of cases (86%) show a characteristic pattern of bilateral symmetric involvement of the dentate nuclei, vestibular nuclei, tegmenta, and superior olivary nuclei. A lack of enhanced lesions with T2-weighted and FLAIR hyperintensity is the most common finding. However, not all cases affect the dentate nuclei, with some cases demonstrating periventricular white matter involvement or affecting the splenium (ATL and reversible splenial lesion [RSL]–like appearance), sparing the dentate nuclei (35,36).

It is important to note if T2 hyperintensity of the dentate nuclei occurs in patients undergoing treatment of tuberculosis with isoniazid, which occurs mainly in countries where tuberculosis is an endemic infection. MR images obtained in this population may show a pattern similar to that of metronidazole-induced brain toxicity (37). Calcium metabolism disorders can manifest calcifications involving the dentate nuclei (2).

Methyl Bromide–induced Toxicity

Methyl bromide is one of the most common components used in pesticides and is usually involved in toxicity related to directed occupational inhalation in agricultural use (38). Methyl bromide–induced toxicity usually manifests with symptoms that are delayed months after initial exposure and are characterized by cranial neuropathy, pyramidal tract dysfunction, and behavioral changes. On T2-weighted and FLAIR images, bilateral symmetric reversible hyperintensities involving the cerebellum and the brainstem can be visualized, including mainly the periaqueductal midbrain, dorsal pons, and dentate nuclei (Fig 13). These imaging findings have a pattern similar to those of WE and metronidazole-induced brain toxicity (38).

Figure E2 summarizes the disorders associated with pattern 2.

Pattern 3: Prominent Cortical Involvement

Adult Hypoglycemic Encephalopathy

Adult hypoglycemic encephalopathy or hypoglycemic brain injury is caused by an imbalance between supply and use of glucose by cerebral cells, leading to brain injury (39). The clinical manifestation is characterized by seizures, a depressed level of consciousness, and even coma in patients

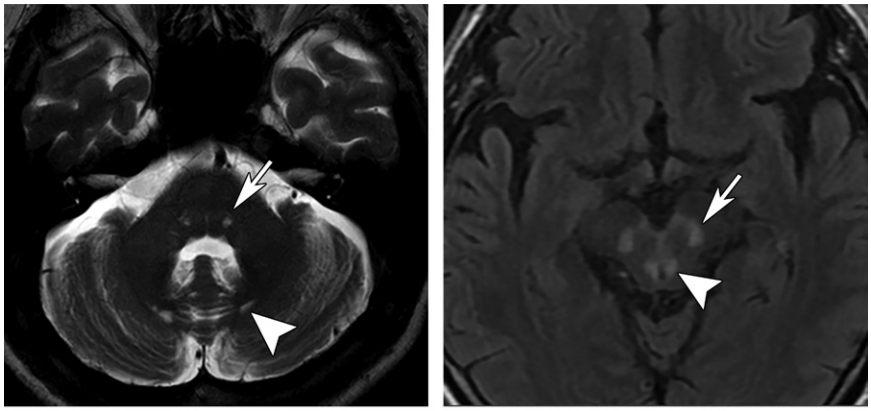

Figure 13. Methyl bromide–induced toxicity. **(a)** Axial T2-weighted MR image shows symmetric hyperintensities involving the dentate nuclei (arrowhead) and dorsal pons (arrow). **(b)** Axial FLAIR MR image shows high-signal-intensity abnormalities involving the periaqueductal gray matter (arrowhead) and subthalamic nuclei (arrow).

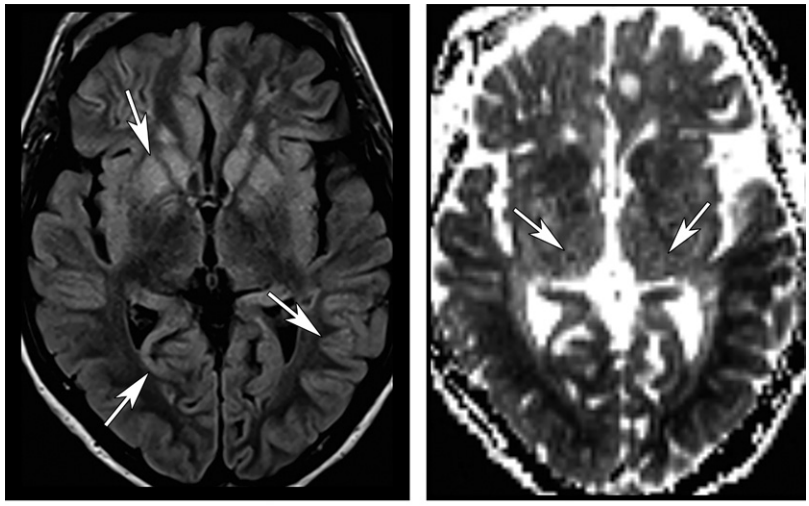

Figure 14. Hypoglycemia in a man with cirrhosis who presented in a coma with a glucose level of 20 mg/dL. **(a)** Axial FLAIR MR image shows symmetric hyperintensities involving the temporal and parieto-occipital cortex and the basal ganglia (arrows) and sparing the white matter and thalami. **(b)** Axial apparent diffusion coefficient (ADC) map shows true restricted diffusion (hypointensity) affecting the same regions and better depicts the thalamic sparing (arrows).

with diabetes (commonly in those patients undergoing insulin replacement therapy) (2,39).

Hypoglycemic encephalopathy has a predilection for posterior and deep regions. The most common imaging findings are symmetric hyperintensities on T2-weighted and FLAIR images and strong restricted diffusion affecting the gyri in the parieto-occipital and temporal regions on diffusion-weighted images. The basal ganglia can be involved, and this involvement may point to poor outcomes. Another suggestive characteristic finding is the sparing of the thalami, white matter, and cerebellum (Fig 14). Earlier signs are better depicted on T1-weighted images as sulcal effacement owing to gyral swelling and can be visualized on CT images as hypoattenuation (2,39).

In newborns, the most common cause is maternal diabetes, which usually manifests in the first 3 postnatal days. The most characteristic pattern of neonatal hypoglycemia is symmetric posterior parieto-occipital gray and white matter signal abnormality with diffusion restriction involving the optic radiations and frequently the posterior thalami (2,40).

An important differential diagnosis for hypoglycemic injury is hypoxic-ischemic brain injury, which has similar imaging findings to those of hypoglycemic encephalopathy. An important piece of information that may help narrow the differential diagnosis is that hypoxic-ischemic brain injury usually manifests with a history of cardiac arrest and usually involves the thalami and cerebellum symmetrically (2,39).

Hyperammonemic Encephalopathy and AHE

Hyperammonemic encephalopathy is primarily caused by hyperammonemia, which has a direct toxic effect on the brain and causes osmotic imbalance (which can lead to ODS) (2,32,41,42). Acute liver failure is the major cause of hyperammonemia, sometimes called AHE (caused by viral infections and other acute hepatic dysfunctions or by AHE superimposed with chronic hepatic failure), but it can manifest in nonhepatic conditions, the most important of which are drug toxicities (valproate and acetaminophen), sepsis, bone marrow transplant, and parenteral nutrition.

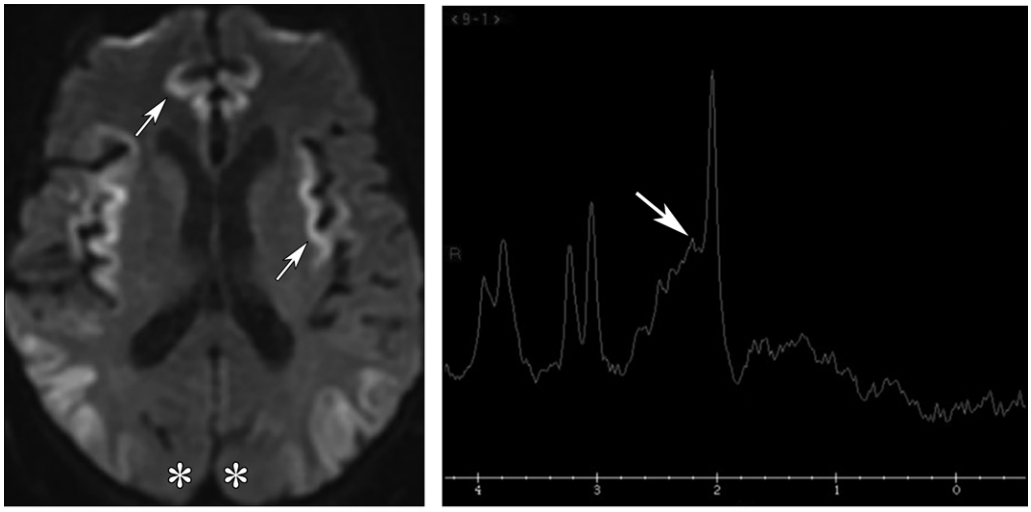

a. b.

Figure 15. Hyperammonemic encephalopathy in a 54-year-old man on the 10th day after liver transplant. **(a)** Axial diffusion-weighted MR image shows bilateral and symmetric restricted diffusion affecting the insular and cingulate gyri (arrows) and sparing the parieto-occipital region (*). **(b)** MR spectroscopic image with an echo time of 30 msec shows a glutamine-glutamate peak at approximately 2.1–2.4 ppm (arrow).

Additionally, such patients usually have a serious condition and other metabolic-associated disorders, such as hypoglycemia and osmotic imbalance, exacerbating brain injury. Rapid recognition and treatment are fundamental for improved patient outcome (32,41,42). Early symptoms can be observed with plasma ammonia levels of 60 μmol/L. Lethargy and vomiting progress to seizures and coma (2,42).

Classic and suggestive imaging characteristics related to hyperammonemic encephalopathy are characterized by strongly restricted diffusion on diffusion-weighted images, accompanied by high signal intensity symmetrically and bilaterally in the insular and cingulate gyri on T2-weighted and FLAIR images (Fig 15a), with relative sparing of the occipital lobes and perirolandic region. The basal ganglia are usually also affected, but hemispheric white matter is typically preserved. Hyperammonemic encephalopathy (owing to AHE or other causes) most commonly involves the insula and thalami (42,43).

Another characteristic finding at MR spectroscopy with short echo times is a glutamate-glutamine peak resonating between 2.1 and 2.4 ppm (Fig 15b). As in cases of chronic hepatic encephalopathy, an increase in glutamine levels is a response to hyperammonemia as glutamine is used to metabolize ammonia (32,33,42).

Less severe cases of AHE with lower ammonia serum levels can manifest at imaging without affecting the cortex and with T2-weighted and FLAIR as well as DWI changes involving the thalami, posterior limb of the internal capsule, and dorsal brainstem, with variable periventricular white matter involvement. It seems that there is a strong correlation between MRI severity and serum ammonia levels and between serum ammonia levels and clinical outcomes (cortical involvement results in more severe cases and with poor outcomes) (34). Note that AHE is a described cause of ATL, manifesting as solely symmetric periventricular white matter involvement, which occurs in 15% of cases (43). After therapy, clinical features and abnormalities at MR spectroscopy improve first, followed 3–6 months later by possible normalization of the signal intensity in the basal ganglia and cortex (32,41,42).

Figure E3 summarizes the disorders associated with pattern 3.

Pattern 4: Symmetric Periventricular White Matter Involvement

Heroin Toxic Leukoencephalopathy

Heroin is an opioid that is most commonly used as a recreational drug for its euphoric effects. This substance is also the most commonly abused opioid and one of the most common drugs used in overdose-related deaths worldwide (2,44,45). Heroin is typically injected intravenously. However, it can also be inhaled. Symptoms usually have rapid onset and last for hours (2,44).

The most common acute complication of injected heroin is stroke, typically involving the globi pallidi (up to 10% of cases), which has a similar imaging manifestation to that depicted in cases of carbon monoxide poisoning (2,45,46). Nonetheless, the most dramatic acute effects occur with inhaled heroin. The freebase form is heated on aluminum foil, and the vapors are inhaled (commonly known as *chasing the dragon*)

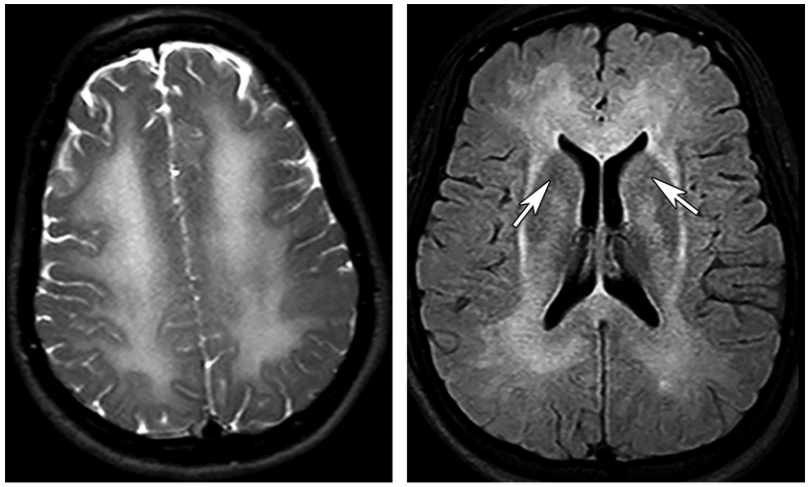

Figure 16. Inhaled heroin (chasing the dragon) toxicity in two patients. **(a)** Axial T2-weighted MR image shows confluent symmetric hyperintensity in the cerebral white matter. Diffusion-weighted images and ADC maps showed restricted diffusion (not shown), and 6-month control images showed normalization (not shown). **(b)** Axial FLAIR MR image in another patient shows bilateral and symmetric hyperintensity affecting the periventricular white matter, with selective involvement of the posterior limb of the internal capsule and sparing of the anterior limb of the internal capsule (arrows).

(2). Toxic leukoencephalopathy related to this method of inhalation has a nonlinear progression and can have a latent period before onset. The disease continues to progress for up to 6 months after cessation of heroin use (2,44,45).

Heroin toxic leukoencephalopathy manifests as confluent, widespread, bilateral, symmetric white matter T2-weighted and FLAIR hyperintensities involving both the supra- and infratentorial compartments (Fig 16). Supratentorial white matter hyperintensities often selectively involve the posterior limb of the internal capsule and periventricular white matter, usually sparing the anterior limb of the internal capsule and subcortical U fibers (Fig 16b). The basal ganglia are rarely involved. Cerebellar involvement manifests as symmetric white matter hyperintensities with dentate nuclei sparing, a pattern sometimes described as a butterfly-wing pattern. Diffusion-weighted images show diffusion restriction in the affected areas during the acute phase (44,45).

Methotrexate and Other Chemotherapeutic Agents

Methotrexate has been associated with CNS toxic effects and the development of leukoencephalopathy after its administration. The general incidence is approximately 0.8%–4.5%, but there are some described risk factors that can elevate these rates, such as intrathecal administration (the major risk factor, with some studies reporting a relative risk of 66%) and high doses (the higher the dose, the higher the risk). Methotrexate-related toxic leukoencephalopathy is most common in pediatric patients (47–49).

There are three main patterns that are classically described for methotrexate-related CNS toxicity: *(a)* toxic leukoencephalopathy, *(b)* disseminated necrotizing encephalopathy, and *(c)* subacute combined degeneration. This final pattern is related to vitamin B12 deficiency, which is addressed further in the article (47–49).

Methotrexate-related toxic leukoencephalopathy is the most common manifestation, with a wide range of clinical and imaging findings. This condition often manifests acutely between 2 and 14 days after methotrexate administration, but manifestation can occur on a delay, even years after use (43–45). The majority of patients are asymptomatic, and imaging findings are mild and transient (47).

The most important imaging finding is true diffusion restriction, bilaterally asymmetric across multiple vascular territories, affecting the centrum semiovale and sparing the subcortical U fibers. These changes are thought to be early signs of acute toxic methotrexate-related leukoencephalopathy (Fig 17a, 17b). The same regions appear on T2-weighted and FLAIR images as hyperintensities and can disappear or persist after symptom resolution (47–49).

Disseminated necrotizing encephalopathy is a rare manifestation and complication of intrathecal methotrexate therapy combined with whole-brain radiation therapy but has more aggressive findings and consequences and is typically fatal (47,49). Clinically, necrotizing encephalopathy is characterized by rapidly progressive subcortical dementia with motor and autonomic deficits (urinary incontinence, gait disturbance, memory difficulty, and hemiparesis) (47,49). MR images show extensive white matter involvement, with multiple low-signal-intensity foci within the disseminated areas of T2 hyperintensity (pointing to hemorrhage). The low-signal-intensity foci have peripheral or solid enhancement, as they are associated with mass effect (tumorlike pattern) (Fig 17c–17e) (47). Lesions and enhancement can disappear completely without any treatment. No reliable imaging features are described to differentiate necrotizing encephalopathy from a recurrent

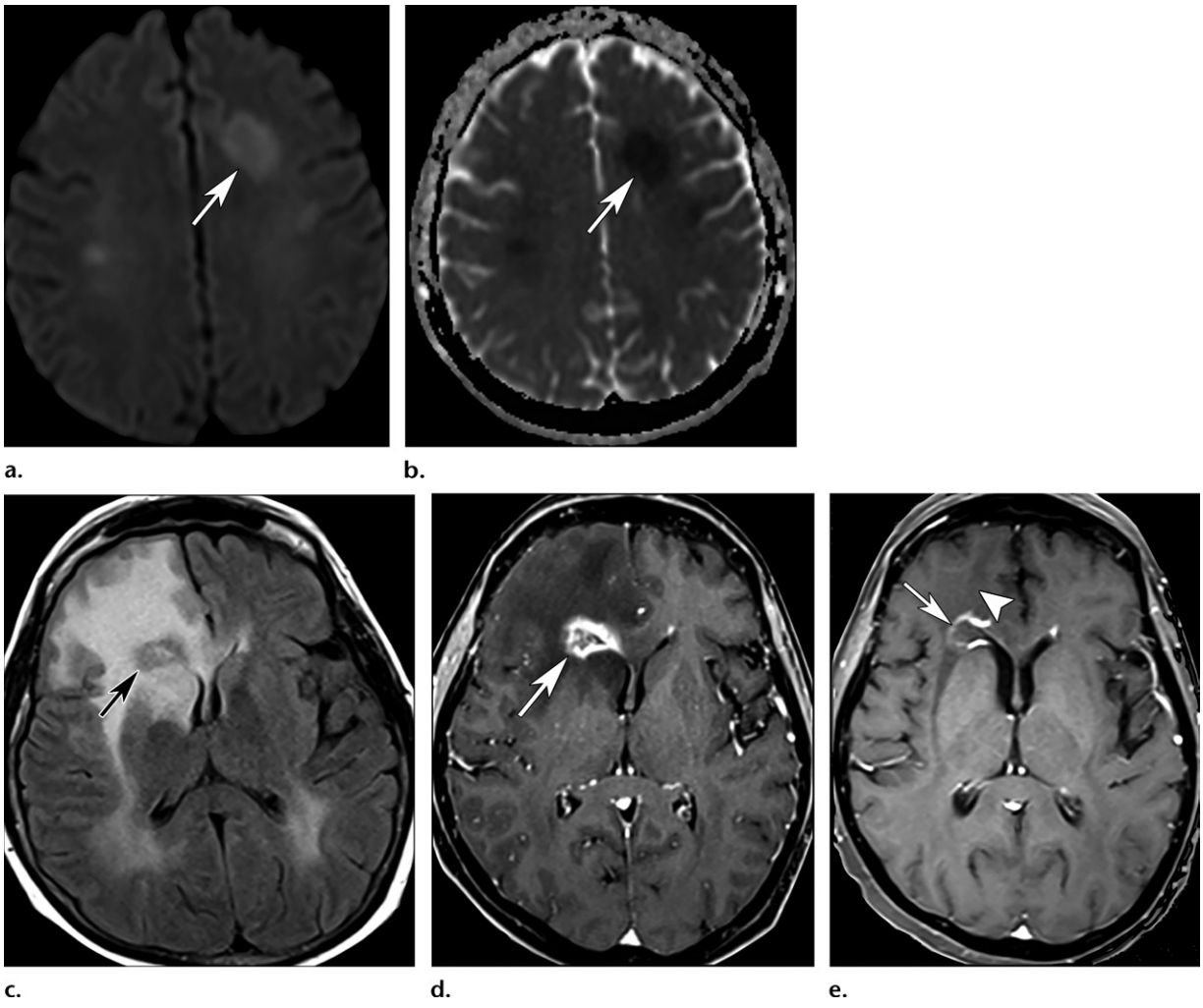

Figure 17. Methotrexate-related CNS toxicity in two patients. **(a, b)** Axial diffusion-weighted image **(a)** and ADC map **(b)** in a patient with toxic leukoencephalopathy show multiple lesions (arrow) with true restricted diffusion affecting the centrum semiovale and crossing vascular territories while sparing the subcortical U fibers. **(c)** Axial FLAIR MR image in another patient with a more severe case of necrotizing encephalopathy after undergoing intrathecal methotrexate therapy combined with whole-brain radiation therapy shows a hypointense lesion (arrow) involved by an extensive confluent area of vasogenic edema (hyperintensity). **(d)** Axial contrast-enhanced T1-weighted MR image in the same patient as in **c** shows peripheral enhancement of the lesion (arrow) and a circumjacent hypointense area of edema. **(e)** Axial contrast-enhanced T1-weighted control MR image obtained 3 months later shows a reduction in the lesion enhancement (arrow) and surrounding edema (arrowhead).

mass, but knowledge or suspicion of this condition prevents unnecessary invasive therapies (49).

Importantly, it is necessary to emphasize that many other chemotherapeutic and immunosuppressive drugs can cause leukoencephalopathy with reversible restricted diffusion (ATL), such as cyclosporine, 5-fluorouracil, and fludarabine (Fig 18). The use of chemotherapeutic agents is the major cause of ATL, and immunosuppressive agents are another group of drugs usually involved with such conditions. The most important pattern to recognize is bilateral symmetric white matter involvement (8,9,43).

Carbon Monoxide Poisoning

Brain toxic effects of carbon monoxide poisoning can appear in a subacute manifestation weeks after initial insult as delayed leukoencephalopathy (ATL) with restricted diffusion and posterior reversibility. Up to one-third of cases demonstrate such findings (Fig 5). All aspects of carbon monoxide poisoning (15) are discussed earlier in this article.

Uremic Encephalopathy

Up to 10% of cases of uremic encephalopathy, discussed previously, can manifest as a classic cause of ATL at imaging, with confluent bilateral and symmetrical periventricular white matter involvement and posterior normalization on follow-up images (19,43).

Acute Hepatic Encephalopathy

As discussed previously, AHE is a cause of ATL in up to 15% of cases, manifesting solely as symmetric periventricular white matter involvement.

AHE is the third most common cause of ATL in a series of 101 cases (43).

Pattern 5: Corticospinal Tract Involvement

Cobalamin Deficiency

Cobalamin deficiency, or vitamin B12 deficiency, can have many causes, such as insufficient intrinsic factor (pernicious anemia, atrophic gastritis, or gastrectomy), ileal malabsorption (Crohn disease, resection of ileum, and infective ileitis), malnutrition (alcohol excess, veganism, and strict vegetarianism), and prolonged use of some medications, such as H2-receptor histaminergic antagonists, metformin, proton pump inhibitors, and methotrexate (50,51). Vitamin B12 deficiency is usually associated with both megaloblastic anemia and subacute combined degeneration. Neurologic symptoms can precede anemia and may not completely resolve after treatment (50,51).

Subacute combined degeneration selectively affects the dorsal and lateral spinal cord columns, depicted as hyperintensities symmetrically affecting such sites at T2-weighted imaging (Fig 19a). The selective involvement of the dorsal columns creates a characteristic appearance of an inverted V shape. With indistinguishable clinical and imaging findings, the less common copper deficiency is a differential diagnosis for subacute combined degeneration. Excessive zinc intake can produce secondary copper deficiency, leading to the same manifestation. Imaging alterations in the brain are nonspecific but are characterized by bilateral hyperintensities on T2-weighted and FLAIR images following the path of the corticospinal tract (Fig 19b) (50,51). Usually there is complete resolution within 3 months after treatment, and permanent residual functional deficit occurs in only a minority of cases (51).

Chronic Hepatic Encephalopathy

Chronic hepatic encephalopathy, discussed previously, is classically recognized by its alterations at T1-weighted imaging. Recent studies show that this condition can lead to the development of variable vasogenic brain edemas during the disease course. It usually affects the white matter in the corticospinal tract regions, most likely due to glutamine accumulation within brain tissue (Fig 11b) (32).

Pattern 6: Corpus Callosum Involvement

Marchiafava-Bignami Disease

MBD is a rare disorder characterized by osmotic demyelination and subsequent necrosis of the corpus callosum. Such conditions are primarily associated with chronic ethanol use and vitamin B complex deficiency (not exclusively B1 deficiency, as in cases of WE) (2,52,53).

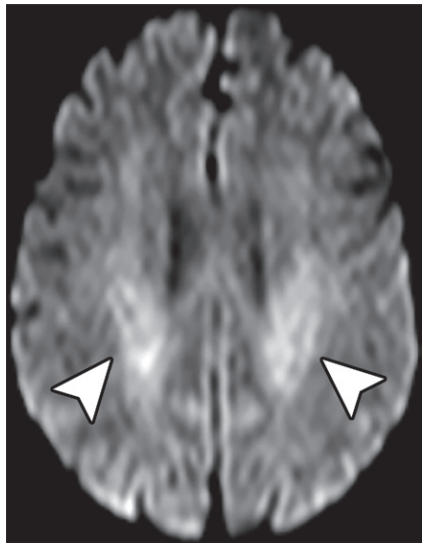

Figure 18. Fludarabine-related toxicity leading to ATL. Axial diffusion-weighted MR image shows symmetric restricted diffusion (arrowheads) involving the periventricular white matter.

MBD manifests in two clinical forms. The first is type A (acute), in which patients present with seizures and or in a coma, with involvement of the entire corpus callosum, and which usually progresses to death within several days. The second is type B (chronic), in which patients are diagnosed with mild encephalopathy and focal lesions in the corpus callosum (most commonly in the genu). MBD is usually accompanied by other alcohol-related pathologic conditions, with some reports of WE and MBD occurring together. Associated brain volume loss is common (52,53).

The diagnosis of MBD at imaging is based on corpus callosum involvement. Selective involvement of the middle layers of the corpus callosum in the context of chronic ethanol use is a highly suggestive finding of MBD. The initial changes associated with acute MBD are best visualized on sagittal FLAIR images. Central callosal involvement sparing the periphery is referred to as the sandwich sign (Fig 20a). Alterations in cases of type B appear first in the genu and frontoparietal cortex followed by splenial involvement. There is variable white matter involvement (53). DWI is initially negative, with diffusion restriction occurring later. Acute lesions may show contrast enhancement (2). Chronic MBD appears as thinning of the corpus callosum with central linear hypointensities on T1-weighted images. Diffusion-tensor images show a reduction in callosal fibers (Fig 20b) (2,52,53).

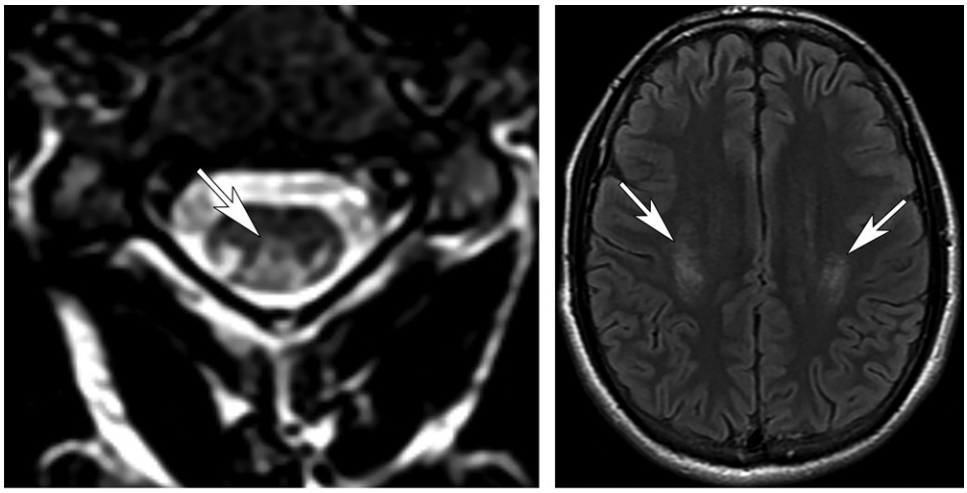

a. b.

Figure 19. Cobalamin deficiency with combined subacute degeneration of the spinal cord. **(a)** Axial T2-weighted MR image of the cervical spine shows involvement of the dorsal and lateral columns (arrow) in an inverted V shape. **(b)** Axial FLAIR MR image of the head shows bilateral hyperintensities (arrows) involving the region of the corticospinal tract.

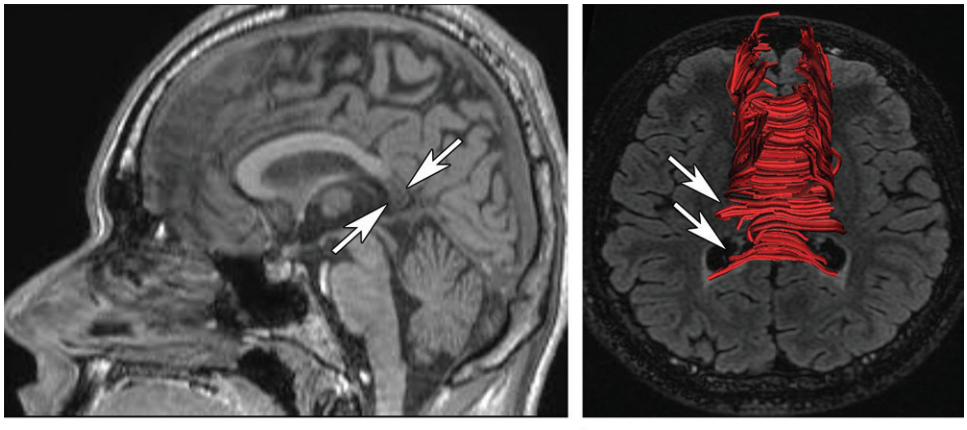

a. b.

Figure 20. MBD in a 30-year-old man with a history of multiple binge drinking episodes who presented with apraxia, hemialexia, and symptoms of dementia. **(a)** Sagittal FLAIR MR image shows demyelinating and necrosis of the central portion of the splenium (hypointensity), sparing the periphery (arrows) (sandwich sign). **(b)** Axial diffusion-tensor reconstructed MR image shows reduction in the callosal fibers (red area) in the same splenial region (arrows).

Reversible Splenial Lesion

The so-called RSLs or cytotoxic lesions of the corpus callosum, which are secondary lesions that are associated with several different entities, are an important imaging differential diagnosis for MBD. These lesions are usually reversible and involve the splenium of the corpus callosum (2,8,9,43,54). The precise pathophysiology of RSLs is unknown but is probably due to excitotoxic intracellular and/or intramyelinic edema, as the splenium has a high density of excitatory receptors that render it vulnerable to cytotoxic edema (2,9,54).

The use and subsequent withdrawal of antiepileptic drugs is most commonly associated with RSLs, which typically manifest between 24 hours and 3 weeks after drug discontinuation. Aside from that, other conditions related to RSLs are viral infection (mild encephalopathy with RSL) and metabolic abnormalities (hypoglycemia, hypernatremia, and acute alcohol poisoning), although there are many other related causes and withdrawal from other types of drugs can lead to RSLs (2,8,9,43,54).

Patients are often asymptomatic, a different clinical presentation from those patients with MBD. Imaging findings include ovoid lesions involving the central splenium, hyperintense lesions on T2-weighted and FLAIR images, and hypointense lesions on T1-weighted images, with restricted diffusion and no enhancement (Fig 21) (2,8,9,54). RSL is considered a subtype of ATL because there is an overlap of

causes between these two entities and owing to its appearance with reversible restricted diffusion. RSL appears to be the mildest severity of ATL, only involving the splenium and with complete posterior resolution (43). The lesions are not always strictly splenial and can involve the entire corpus callosum in a minority of cases. In addition, patients can be diagnosed with severe encephalopathy and sometimes the lesion is not completely reversible, which is why the use of the term *cytotoxic lesions of the corpus callosum* is currently preferred (55).

Figure E4 summarizes the disorders associated with patterns 4, 5, and 6.

Pattern 7: Asymmetric White Matter Involvement (Demyelinating Disease Pattern)

Levamisole-induced Leukoencephalopathy

Levamisole is a medication with anthelmintic and immunomodulatory properties, but its use has been suspended in most countries because of its collateral effects. It has been recognized as a cocaine adulterant because it can induce effects similar to those of cocaine on the CNS. It is estimated that approximately 69% of commercialized cocaine worldwide is adulterated (56–58). Patients are usually adolescents or young adults and present with a strokelike episode, which makes it an important differential diagnosis in this population and affects patient management (56,57).

Imaging characteristically shows lesions with a tumefactive demyelinating pattern, represented as one or a few randomly distributed oval or round lesions in the centrum semiovale, with no mass effect or edema, with smooth and incomplete enhancement peripherally (C-shaped appearance, the incomplete portion is related to the cortex) and strongly restricted diffusion (Fig 22). T2-weighted and diffusion-weighted images can depict concentric layers of hyperintensities. Another important characteristic is that after treatment with steroids, lesions tend to regress and even disappear. Recognizing this entity is of great importance in guiding management approaches and treatment (56–58).

One should remember the important well-known and extensively described intracranial vascular effects of cocaine and of many other illicit drugs. Blood pressure imbalance induces ischemic and/or hemorrhagic stroke or even reversible cerebral vasoconstriction syndrome and PRES (46).

Chemotherapeutic Agents

Many chemotherapeutic agents have been related to neurotoxic effects and induce a demyelinating leukoencephalopathy pattern during the course of treatment, characterized at imaging as multiple ovoid asymmetric white matter hyperintensities in a perivenular distribution (59). The most common agents related to this pattern are tumor necrosis factor-α blockers (infliximab, adalimumab), which are currently widely used to treat immune-mediated conditions and some cancers (59). Vincristine, a chemotherapeutic agent used to treat some types of leukemia, Hodgkin disease, and small cell lung cancer, has also been associated with this pattern of neurotoxicity (59).

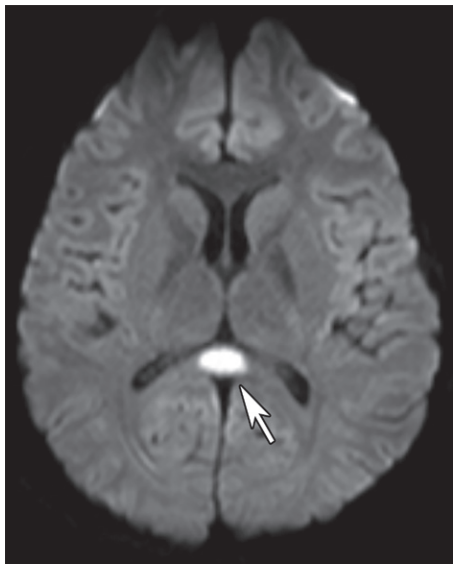

Figure 21. Ovoid lesion in a patient who presented to the emergency department after using a large amount of cannabis. No abnormal symptoms other than those that are expected after cannabis use were seen. Axial diffusion-weighted MR image shows a single ovoid central lesion (arrow) affecting the splenium, with true restricted diffusion (ADC map not shown). MRI (not shown) performed months later was normal.

Pattern 8: Parieto-occipital Subcortical Vasogenic Edema

Posterior Reversible Encephalopathy Syndrome

PRES, also known as *reversible posterior leukoencephalopathy syndrome*, refers to a clinicoradiologic disorder of potentially reversible subcortical vasogenic brain edema in patients with classic acute neurologic symptoms (seizure in 60%–75%, altered mental function and headache in 20%–25%) in the setting of several conditions, such as hypertension, preeclampsia, renal failure, sepsis, thrombocytopenia, the administration of cytotoxic or immunosuppressive medications, and many other potential causes. Symptoms and imaging findings usually normalize after treatment (2,60–62).

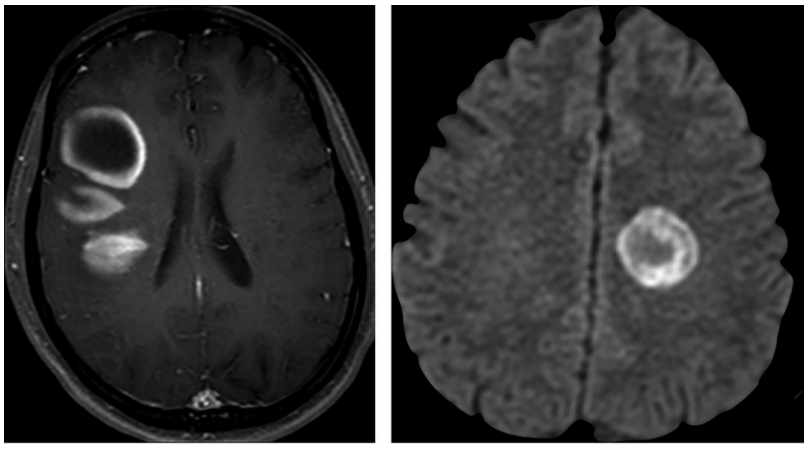

Figure 22. Levamisole-induced leukoencephalopathy in two patients. **(a)** Axial contrast-enhanced T1-weighted MR image shows hypointense lesions within the centrum semiovale with incomplete peripheral enhancement, without edema or mass effect. **(b)** Axial diffusion-weighted MR image shows a lesion centered in the centrum semiovale with strong restricted diffusion and different concentric layers of hyperintensities. Both cases depict lesions with a tumefactive demyelinating pattern.

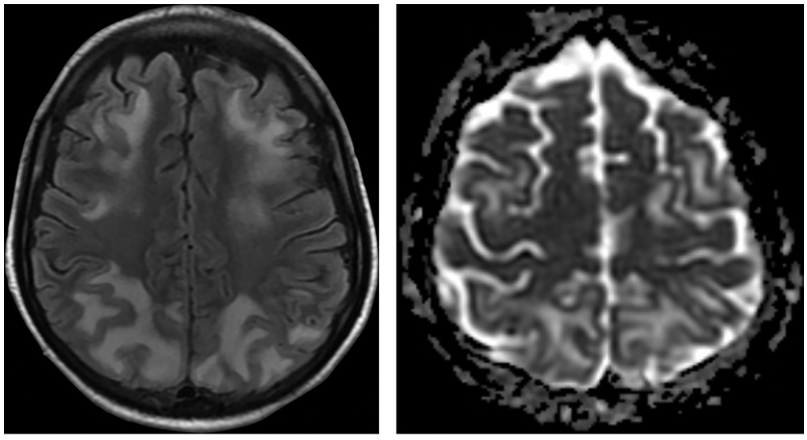

Figure 23. PRES. **(a)** Axial FLAIR MR image shows bilateral asymmetric hyperintensity involving the subcortical white matter of the parieto-occipital and frontal lobes, sparing the cortex. **(b)** Axial ADC map shows no true restricted diffusion affecting these areas, indicating a vasogenic edema mechanism. A postcontrast T1-weighted MR image (not shown) showed no enhancement. Such findings are compatible with vasogenic edema in a typical PRES distribution. Clinical and epidemiologic findings can favor this diagnosis.

PRES was classically described as a cerebrovascular autoregulatory disorder caused by hypertension, but this pathophysiologic theory does not explain the manifestation of all the clinical and imaging findings. In addition, most patients present with only mild blood pressure elevation, and 20%–30% of patients are normotensive. Current theories have a similar shared mechanism, advocating endothelial injury and dysfunction secondary to different causes (cytotoxic, immunogenic), ultimately resulting in vasogenic edema. Interstitial fluid accumulates in the subcortical white matter, with a predilection for the parietal and occipital lobes (2,61,62). This condition occurs at all ages but is most common in young women (2).

Imaging findings include changes associated with vasogenic edema, commonly bilateral and asymmetric high signal intensity on T2-weighted and FLAIR images and hypoattenuation on CT images involving the subcortical white matter (Fig 23). Diffusion-weighted images and apparent diffusion coefficient maps are often negative (differentiating the condition from cytotoxic and intramyelinic edema) or at least have a smaller extension than those changes depicted on FLAIR images. Postcontrast enhancement is not a typical feature, but some studies report that up to 37% of cases depict contrast enhancement (61,62).

Proposed algorithms for PRES diagnosis usually involve the presence of suggestive clinical symptoms associated with known risk factors and typical imaging findings (61).

There are many patterns of involvement that have been described, including *(a)* parieto-occipital involvement, the most common and suggestive pattern (up to 90%, also known as *classic PRES*); *(b)* the superior frontal sulcus pattern (70%); *(c)* the holohemispheric watershed pattern (50%); and *(d)* involvement in other less common sites, such as the cerebellum, basal ganglia, and brainstem (2). Combinations of patterns are common (more than 90% of cases). Note that PRES, despite its name, is not always reversible and not always posterior (2,61,63).

Prompt suspicion and recognition of PRES is important because delayed diagnosis can progress to subarachnoid hemorrhage and/or infarction owing to diffuse vascular contraction secondary to endothelial dysautoregulation (2,61–63).

The administration of many drugs can lead to PRES or PRES-like symptoms and imaging presentation, the most important of which are cyclosporine and tacrolimus. An important tip is that in these drug-related cases, an atypical PRES is the rule, with symmetric lesions in unusual sites and possible contrast enhancement at imaging (61–63).

Pattern 9: Symmetric Central Pontine Involvement

Osmotic Demyelination Syndrome

ODS is an acute form of demyelination caused by rapid shifts in serum osmolality. The classic and most common cause is a rapid correction of hyponatremia. However, it is important to remember that ODS may occur in patients who are normonatremic. In fact, this heterogeneous disorder has osmotic stress as its basic cause. Many other conditions that lead to ODS have been described, and there are known comorbid conditions that predispose patients to its development. These causes and predisposing conditions are described in Table 3 (2,64).

In the classic context of rapid hyponatremia correction leading to ODS, sodium levels are usually lower than 115 mmol/L, and correction rates are higher than 12 mmol/L per day (2).

Oligodendrocytes are especially vulnerable to osmotic changes (particularly at the pons) leading to demyelination that most commonly involves the brainstem region, which is why this entity was classically called *central pontine myelinolysis*. Nevertheless, any brain cell can be affected by osmotic imbalance, and ODS affecting extrapontine cerebral regions, including the cortex, has been extensively described. Approximately 50% of cases manifest isolated pontine lesions, with pontine and extrapontine lesions in 30% of cases. There are only extrapontine lesions in 20% of ODS cases, which makes diagnosing this condition even more challenging and underscores the importance of recognizing the spectrum of ODS symptoms (2,64,65).

The main signs or symptoms are seizures and altered mental status, often biphasic, with altered mental status when hyponatremia has manifested and subsequent improvement after natremia restoration followed by new rapid deterioration after approximately 1 week (2,64).

The classic and most common imaging appearance consists of well-demarcated and symmetric, rounded, or trident-shaped lesions on the central pons that characteristically spare the peripheral pons and corticospinal tract regions (Fig 24a). Sparing of the transverse pontine fibers is described and can be visualized at imaging as fine lines of normal signal intensity crossing the lesion. Alterations are depicted on conventional images 1–2 weeks after symptom onset as a hypoattenuating lesion on CT images, a hypointense lesion on T1-weighted images, and a hyperintense lesion on T2-weighted and FLAIR images. Importantly, diffusion-weighted images can depict restricted diffusion in the acute phase as soon as 24 hours after the onset of ODS, which is an important finding for early diagnosis (2,64,65).

Table 3: Causes and Predisposing Conditions of ODS

Causes
Rapid hyponatremia correction
Alcoholism
Liver transplant (hyperammonemia)
Malnutrition
Hyper- or hypoglycemia
Azotemia and hemodialysis
Predisposing conditions
Renal, adrenal, and pituitary disease
Hyperemesis
History of transplantation
Severe burns
Prolonged use of diuretics
Paraneoplastic disease

The most commonly involved extrapontine sites are the basal ganglia, thalami, and hemispheric white matter, often symmetrically. Some cases show laminar necrosis of the cortex (2,64). There is an uncommon but suggestive manifestation of extrapontine ODS. Studies have shown that the white matter immediately underlying the gray matter is especially susceptible to osmotic distress, leading to alterations in these sites that are depicted on images as multiple and diffuse punctate lesions on juxtacortical white matter or delineating the transition line between cortical gray matter and subjacent white matter (Fig 24b) (65).

Suggestive Sites of Involvement

Some sites of involvement more specifically suggest a reduced number of conditions and may point to subjacent diagnoses (Fig 25). Remember that most findings are not pathognomonic. However, by considering the patient's clinical history, it is possible to reduce the number of conditions in the differential diagnosis. These correlations refer only to toxic and metabolic causes and can be used for orientation in a suitable clinical context.

Conclusion

Diagnosing toxic and metabolic brain disorders remains challenging and refers to a heterogeneous group of diseases. Although many imaging manifestations are unspecific, some imaging

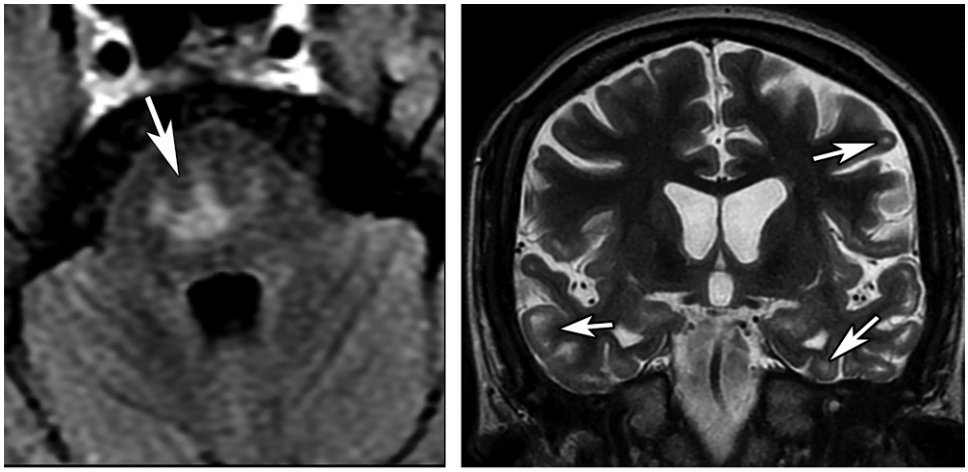

a. b.

Figure 24. ODS in two patients. **(a)** Axial FLAIR MR image shows classic findings of ODS, characterized by a trident-shaped lesion (arrow) affecting the central pons and sparing of the periphery and the region of the corticospinal tract. **(b)** Coronal T2-weighted MR image with extrapontine findings shows multiple juxtacortical (white matter–gray matter transition) hyperintense lesions (arrows).

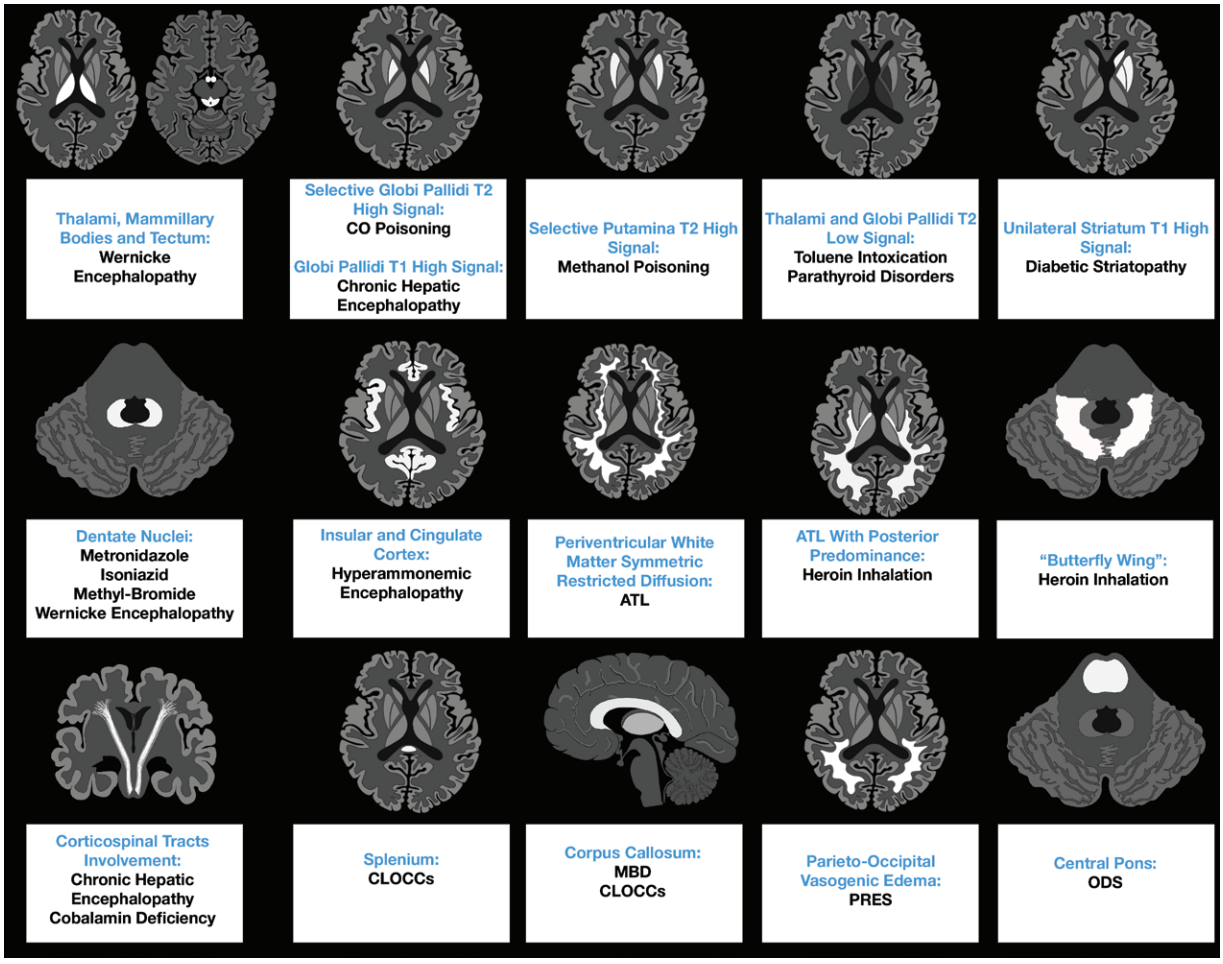

Figure 25. Chart demonstrates the correlation between more specific sites of involvement in toxic and metabolic brain disorders and their most likely diagnoses. *CLOCCs* = cytotoxic lesions of the corpus callosum, *CO* = carbon monoxide.

findings can be quite specific for a few conditions. Nonetheless, some prognostic information can be obtained from imaging studies, suggesting a reversible subjacent cause or indicating severe involvement of cerebral structures.

Approaching these conditions by considering the patterns at imaging can add to the radiologist's daily routine. Depending on the pattern, pathophysiologic information can be inferred and a reduced number of conditions in the differential diagnosis can be considered.

Many other causes related to toxic and metabolic disorders exist, and there are other possible uncommon presentations for each cause. The proposed patterns and online supplements describe the majority of the most common conditions and presentations encountered in clinical practice and can be helpful when diagnosing such a group of diseases. One should always look for the accessible clinical history as it points to subjacent toxic and metabolic causes over other groups of diseases that can show the same imaging characteristics. Combining clinical issues with imaging findings can make it possible to reach a specific diagnosis.

***Disclosures of Conflicts of Interest.*—A.M.M.** *Activities related to the present article:* disclosed no relevant relationships. *Activities not related to the present article:* chief executive officer of VEEV; payment from VEEV for informatics solutions consulting. *Other activities:* pending informatics patent from Radnosis, VEEV. **L.T.L.** *Activities related to the present article:* disclosed no relevant relationships. *Activities not related to the present article:* payment for a 2017 lecture from Bracco Imaging. *Other activities:* disclosed no relevant relationships.

References

1. Valk J, van der Knaap MS. Toxic encephalopathy. AJNR Am J Neuroradiol 1992;13(2):747–760.
2. Osborn AG, Hedlund GL, Salzman KL. Toxic, metabolic, degenerative and CSF disorders. In: Osborn's Brain. 2nd ed. Philadelphia, Pa: Elsevier, 2017; 905–1155.
3. Schaefer PW, Buonanno FS, Gonzalez RG, Schwamm LH. Diffusion-weighted imaging discriminates between cytotoxic and vasogenic edema in a patient with eclampsia. Stroke 1997;28(5):1082–1085.
4. Na DG, Kim EY, Ryoo JW, et al. CT sign of brain swelling without concomitant parenchymal hypoattenuation: comparison with diffusion- and perfusion-weighted MR imaging. Radiology 2005;235(3):992–998.
5. Lipton SA, Rosenberg PA. Excitatory amino acids as a final common pathway for neurologic disorders. N Engl J Med 1994;330(9):613–622.
6. Moritani T, Smoker WRK, Sato Y, Numaguchi Y, Westesson PL. Diffusion-weighted imaging of acute excitotoxic brain injury. AJNR Am J Neuroradiol 2005;26(2):216–228.
7. Chokshi FH, Aygun N, Mullins ME. Imaging of acquired metabolic and toxic disorders of the basal ganglia. Semin Ultrasound CT MR 2014;35(2):75–84.
8. McKinney AM, Kieffer SA, Paylor RT, SantaCruz KS, Kendi A, Lucato L. Acute toxic leukoencephalopathy: potential for reversibility clinically and on MRI with diffusion-weighted and FLAIR imaging. AJR Am J Roentgenol 2009;193(1):192–206. .
9. Rimkus Cde M, Andrade CS, Leite Cda C, McKinney AM, Lucato LT. Toxic Leukoencephalopathies, Including Drug, Medication, Environmental, and Radiation-Induced Encephalopathic Syndromes. Semin Ultrasound CT MR 2014;35(2):97–117.
10. Santos Andrade C, Tavares Lucato L, da Graça Morais Martin M, et al. Non-alcoholic Wernicke's encephalopathy: broadening the clinicoradiological spectrum. Br J Radiol 2010;83(989):437–446.
11. Kim TE, Lee EJ, Young JB, Shin DJ, Kim JH. Wernicke encephalopathy and ethanol-related syndromes. Semin Ultrasound CT MR 2014;35(2):85–96.
12. Blanco M, Casado R, Vázquez F, Pumar JM. CT and MR imaging findings in methanol intoxication. AJNR Am J Neuroradiol 2006;27(2):452–454.
13. Hegde AN, Mohan S, Lath N, Lim CC. Differential diagnosis for bilateral abnormalities of the basal ganglia and thalamus. RadioGraphics 2011;31(1):5–30.
14. Vaneckova M, Zakharov S, Klempir J, et al. Imaging findings after methanol intoxication (cohort of 46 patients). Neuroendocrinol Lett 2015;36(8):737–744.
15. Sener RN. Acute carbon monoxide poisoning: diffusion MR imaging findings. AJNR Am J Neuroradiol 2003;24(7):1475–1477.
16. Lo CP, Chen SY, Lee KW, et al. Brain injury after acute carbon monoxide poisoning: early and late complications. AJR Am J Roentgenol 2007;189(4):W205–W211.
17. Pearl PL, Vezina LG, Saneto RP, et al. Cerebral MRI abnormalities associated with vigabatrin therapy. Epilepsia 2009;50(2):184–194.
18. Hussain SA, Tsao J, Li M, et al. Risk of vigabatrin-associated brain abnormalities on MRI in the treatment of infantile spasms is dose-dependent. Epilepsia 2017;58(4):674–682.
19. Kim DM, Lee IH, Song CJ. Uremic Encephalopathy: MR Imaging Findings and Clinical Correlation. AJNR Am J Neuroradiol 2016;37(9):1604–1609.
20. Donnerstag F, Ding X, Pape L, et al. Patterns in early diffusion-weighted MRI in children with haemolytic uraemic syndrome and CNS involvement. Eur Radiol 2012;22(3):506–513.
21. Murray AM, Tupper DE, Knopman DS, et al. Cognitive impairment in hemodialysis patients is common. Neurology 2006;67(2):216–223.
22. Kumar G, Goyal MK. Lentiform Fork sign: a unique MRI picture—Is metabolic acidosis responsible? Clin Neurol Neurosurg 2010;112(9):805–812.
23. Aydin K, Sencer S, Demir T, Ogel K, Tunaci A, Minareci O. Cranial MR findings in chronic toluene abuse by inhalation. AJNR Am J Neuroradiol 2002;23(7):1173–1179.
24. Caldemeyer KS, Pascuzzi RM, Moran CC, Smith RR. Toluene abuse causing reduced MR signal intensity in the brain. AJR Am J Roentgenol 1993;161(6):1259–1261.
25. Hurley RA, Taber KH. Occupational exposure to solvents: neuropsychiatric and imaging features. J Neuropsychiatry Clin Neurosci 2015;27(1):1–6.
26. Shoback DM, Bilezikian JP, Costa AG, et al. Presentation of Hypoparathyroidism: Etiologies and Clinical Features. J Clin Endocrinol Metab 2016;101(6):2300–2312.
27. de la Plaza Llamas R, Ramia Ángel JM, Arteaga Peralta V, Hernández Cristóbal J, López Marcano AJ. Brain calcifications and primary hyperparathyroidism. Cir Esp 2016;94(1):e5–e7.
28. Piciucchi S, Barone D, Gavelli G, Dubini A, Oboldi D, Matteuci F. Primary hyperparathyroidism: imaging to pathology. J Clin Imaging Sci 2012;2(1):59.
29. Lai PH, Tien RD, Chang MH, et al. Chorea-ballismus with nonketotic hyperglycemia in primary diabetes mellitus. AJNR Am J Neuroradiol 1996;17(6):1057–1064.
30. Bathla G, Policeni B, Agarwal A. Neuroimaging in patients with abnormal blood glucose levels. AJNR Am J Neuroradiol 2014;35(5):833–840.
31. Alonso J, Córdoba J, Rovira A. Brain magnetic resonance in hepatic encephalopathy. Semin Ultrasound CT MR 2014;35(2):136–152.
32. Rovira A, Alonso J, Córdoba J. MR imaging findings in hepatic encephalopathy. AJNR Am J Neuroradiol 2008;29(9):1612–1621.
33. Ramadan S, Lin A, Stanwell P. Glutamate and glutamine: a review of in vivo MRS in the human brain. NMR Biomed 2013;26(12):1630–1646.
34. Matsusue E, Kinoshita T, Ohama E, Ogawa T. Cerebral cortical and white matter lesions in chronic hepatic en-

cephalopathy: MR-pathologic correlations. AJNR Am J Neuroradiol 2005;26(2):347–351.
35. Kuriyama A, Jackson JL, Doi A, Kamiya T. Metronidazole-induced central nervous system toxicity: a systematic review. Clin Neuropharmacol 2011;34(6):241–247.
36. Kim E, Na DG, Kim EY, Kim JH, Son KR, Chang KH. MR imaging of metronidazole-induced encephalopathy: lesion distribution and diffusion-weighted imaging findings. AJNR Am J Neuroradiol 2007;28(9):1652–1658.
37. Peter P, John M. Isoniazid-induced cerebellitis: a disguised presentation. Singapore Med J 2014;55(1):e17–e19.
38. Geyer HL, Schaumburg HH, Herskovitz S. Methyl bromide intoxication causes reversible symmetric brainstem and cerebellar MRI lesions. Neurology 2005;64(7):1279–1281.
39. Kang EG, Jeon SJ, Choi SS, Song CJ, Yu IK. Diffusion MR imaging of hypoglycemic encephalopathy. AJNR Am J Neuroradiol 2010;31(3):559–564.
40. Wong DS, Poskitt KJ, Chau V, et al. Brain injury patterns in hypoglycemia in neonatal encephalopathy. AJNR Am J Neuroradiol 2013;34(7):1456–1461.
41. McKinney AM, Lohman BD, Sarikaya B, et al. Acute hepatic encephalopathy: diffusion-weighted and fluid-attenuated inversion recovery findings, and correlation with plasma ammonia level and clinical outcome. AJNR Am J Neuroradiol 2010;31(8):1471–1479.
42. U-King-Im JM, Yu E, Bartlett E, Soobrah R, Kucharczyk W. Acute hyperammonemic encephalopathy in adults: imaging findings. AJNR Am J Neuroradiol 2011;32(2):413–418.
43. Özütemiz C, Roshan SK, Kroll NJ, et al. Acute Toxic Leukoencephalopathy: Etiologies, Imaging Findings, and Outcomes in 101 Patients. AJNR Am J Neuroradiol 2019;40(2):267–275.
44. Keogh CF, Andrews GT, Spacey SD, Forkheim KE, Graeb DA. Neuroimaging features of heroin inhalation toxicity: "chasing the dragon". AJR Am J Roentgenol 2003;180(3):847–850.
45. Geibprasert S, Gallucci M, Krings T. Addictive illegal drugs: structural neuroimaging. AJNR Am J Neuroradiol 2010;31(5):803–808.
46. Tamrazi B, Almast J. Your brain on drugs: imaging of drug-related changes in the central nervous system. RadioGraphics 2012;32(3):701–719.
47. Inaba H, Khan RB, Laningham FH, Crews KR, Pui CH, Daw NC. Clinical and radiological characteristics of methotrexate-induced acute encephalopathy in pediatric patients with cancer. Ann Oncol 2008;19(1):178–184.
48. Reddick WE, Glass JO, Helton KJ, et al. Prevalence of leukoencephalopathy in children treated for acute lymphoblastic leukemia with high-dose methotrexate. AJNR Am J Neuroradiol 2005;26(5):1263–1269.
49. Kim JY, Kim ST, Nam DH, Lee JI, Park K, Kong DS. Leukoencephalopathy and disseminated necrotizing leukoencephalopathy following intrathecal methotrexate chemotherapy and radiation therapy for central nerve system lymphoma or leukemia. J Korean Neurosurg Soc 2011;50(4):304–310.
50. Morita S, Miwa H, Kihira T, Kondo T. Cerebellar ataxia and leukoencephalopathy associated with cobalamin deficiency. J Neurol Sci 2003;216(1):183–184.
51. Briani C, Dalla Torre C, Citton V, et al. Cobalamin deficiency: clinical picture and radiological findings. Nutrients 2013;5(11):4521–4539.
52. Tung CS, Wu SL, Tsou JC, Hsu SP, Kuo HC, Tsui HW. Marchiafava-Bignami disease with widespread lesions and complete recovery. AJNR Am J Neuroradiol 2010;31(8):1506–1507.
53. Arbelaez A, Pajon A, Castillo M. Acute Marchiafava-Bignami disease: MR findings in two patients. AJNR Am J Neuroradiol 2003;24(10):1955–1957.
54. Lin D, Rheinboldt M. Reversible splenial lesions presenting in conjunction with febrile illness: a case series and literature review. Emerg Radiol 2017;24(5):599–604.
55. Starkey J, Kobayashi N, Numaguchi Y, Moritani T. Cytotoxic Lesions of the Corpus Callosum That Show Restricted Diffusion: Mechanisms, Causes, and Manifestations. RadioGraphics 2017;37(2):562–576.
56. Yan R, Wu Q, Ren J, et al. Clinical features and magnetic resonance image analysis of 15 cases of demyelinating leukoencephalopathy induced by levamisole. Exp Ther Med 2013;6(1):71–74.
57. Lucia P, Pocek M, Passacantando A, Sebastiani ML, De Martinis C. Multifocal leucoencephalopathy induced by levamisole. Lancet 1996;348(9039):1450.
58. Kemanetzoglou E, Andreadou E. CNS Demyelination with TNF-a Blockers. Curr Neurol Neurosci Rep 2017;17(4):36.
59. Eiden C, Diot C, Mathieu O, Mallaret M, Peyrière H. Levamisole-adulterated cocaine: what about in European countries? J Psychoactive Drugs 2014;46(5):389–392.
60. Stone JB, DeAngelis LM. Cancer-treatment-induced neurotoxicity: focus on newer treatments. Nat Rev Clin Oncol 2016;13(2):92–105.
61. Gao B, Lyu C, Lerner A, McKinney AM. Controversy of posterior reversible encephalopathy syndrome: what have we learnt in the last 20 years? J Neurol Neurosurg Psychiatry 2018;89(1):14–20.
62. McKinney AM, Short J, Truwit CL, et al. Posterior reversible encephalopathy syndrome: incidence of atypical regions of involvement and imaging findings. AJR Am J Roentgenol 2007;189(4):904–912.
63. Rykken JB, McKinney AM. Posterior reversible encephalopathy syndrome. Semin Ultrasound CT MR 2014;35(2):118–135.
64. Alleman AM. Osmotic demyelination syndrome: central pontine myelinolysis and extrapontine myelinolysis. Semin Ultrasound CT MR 2014;35(2):153–159.
65. Tatewaki Y, Kato K, Tanabe Y, Takahashi S. MRI findings of corticosubcortical lesions in osmotic myelinolysis: report of two cases. Br J Radiol 2012;85(1012):e87–e90.